ANTEROLATERAL VERSUS MEDIAL PLATING FOR PILON FRACTURES

ANTEROLATERAL VERSUS MEDIAL PLATING FOR COMMINUTED INTRA-ARTICULAR DISTAL TIBIA FRACTURES: A BIOMECHANICAL ASSESSMENT

By MARISA KOHUT, B.Eng.

A Thesis Submitted to the School of Graduate Studies in Partial Fulfilment of the Requirements for the Degree of Master of Applied Science in Engineering

McMaster University Master of Applied Science in Engineering (2019) Hamilton, Ontario

TITLE: Anterolateral Versus Medial Plating for Comminuted Intra-Articulation Distal Tibia Fractures: A Biomechanical Assessment

AUTHOR: Marisa Kohut, B.Eng.

SUPERVISOR: Dr. Cheryl E. Quenneville, B.Sc., M.E.Sc., Ph.D.

NUMBER OF PAGES: xiv, 90

Lay Abstract

Severe distal tibial fractures (pilon fractures) occur during motor vehicle collisions and falls from a height and are typically treated with one of two fracture fixations. The evidence supporting the use of the fracture fixations is limited and research has yet to be done using cadaveric specimens.

To assess the fracture fixations, six cadaveric specimens were subjected to compressive loading to determine the stiffness. An orthopaedic surgeon then simulated a pilon fracture and repaired each specimen with one of the two fixations. The specimens were then subjected to compressive loading to determine the repaired stiffness and then loaded until failure. During failure testing, an optical tracking system was used to assess the overall motion of the fracture fragments.

Based on preliminary results from stiffness, strength, and relative motion evaluations, the medial plate showed superior results; however, the differences were not found to be statistically significant.

Abstract

Pilon fractures are a result of high energy impacts to the ankle joint causing comminution to the tibia. Open reduction and internal fixation is the current method of treatment, which involves reducing the fracture and placing an anterolateral or medial plate along the tibia to secure the bone fragments during the bone healing process, but these have frequent complications for patients. No previous studies have investigated the biomechanical performance of these plates using a model that consists of the tibia, fibula and the syndesmotic tissue. The purpose of this study was to evaluate the biomechanical effectiveness of these plates using cadaveric specimens.

Eight pairs of cadaveric specimens were anatomically aligned and potted proximally. A typical fracture pattern was created in each specimen and then one from each pair treated with an anterolateral and the other with a medial plate. A materials testing machine applied an axial load to the specimen to determine the construct stiffness, followed by a ramp load to failure. An optical tracking system was configured to track the motion of the bone fragments in 3D space. The medial plates tended to provide superior results when compared to the anterolateral plate; however, no statistical difference was found.

This represents the most complex fracture and comprehensive evaluation of the plating options available for this type of injury and may inform surgeons to help reduce the poor outcomes for patients.

Acknowledgments

Firstly, I would like to thank my supervisor, Dr. Cheryl Quenneville. You have been an exceptional mentor throughout my degree, and I appreciate your support towards my personal and professional goals. Thanks for helping connect all of those dots!

Dr. Bashar Alolabi, it has been a pleasure getting to work with you on my project. I truly enjoyed all of our conversations while working in the lab and at your clinic. Thank you for taking the time to teach me and support my interest in medicine.

Julia de Lange, it has been a pleasure being desk mates, roommates and lab mates over the past two years. I am forever grateful for our friendship and the support you provided over the past two years.

To the rest of my lab group; Cooper, Noah and Fatemeh, you have all been exceptional to work with. Jessica and Ellie, our time testing in the lab together was short, but your help and support made those days easier.

To everyone who helped support me while I took on the challenge of setting up the motion capture system in my lab: Dr. Elizabeth Hassan, Elora Brenneman, Thierry Chevalier, and Dr. Janie Wilson. At times this task seemed like it was bigger than I could chew but, with all of your help, it worked.

Thank you Depuy Synthes for providing the plates to complete this study and the opportunity to learn from them.

To the Mechanical Engineering Department Machine Shop (Mark, Justin, John, Michael and Ron), thank you for sharing all of your great ideas and coaching me while in the shop!

Shout out to my fellow BME students! Forever grateful for all the chats and snacks that happened in the office. Especially, Devon Jones, thank you for keeping me in check and sharing your desk snacks!

My family – Mom, Dad, Rachel, Sam & Madi- although you are all spread out across the country, your support was always only a phone call away.

Lastly, Atli, words aren't enough to describe how grateful I am to have you as a partner. Thank you for reviewing my writing, listening to my practice presentations and showing up to the actual ones. You truly are the best.

Table of Contents

List of Figures

List of Tables

List of Abbreviations and Symbols

$\vec{O}$	Origin Vector
$\vec{P}$	Position Vector
±	Plus/minus
°	Degree
″	Inch
′	Local Coordinate System
%	Percent
$\rightharpoonup$	Vector
3D	Three-dimensional
ANT	Anterolateral
cm	Centimeter
FPS	Frames Per Second
IM	Intramedullary
MED	Medial
mm	Millimeter
N	Newton
ORIF	Open Reduction and Internal Fixation
R	Rotational Matrix
s	Second

Declaration of Academic Achievement

The following is a declaration that I, Marisa Kohut, completed the research described in this thesis and recognize the contributions of Dr. Cheryl Quenneville and Dr. Bashar Alolabi. I contributed to the study, set-up the equipment, performed the experiments, collected the data, processed the data and wrote the manuscript. Dr. Cheryl Quenneville assisted with the study design and review of the manuscript. Dr. Bashar Alolabi contributed to the study design and to the specimen preparation.

Chapter 1: Introduction

1.1 Motivation[1]

Pilon fractures are a type of injury characterized by comminution (fragmentation into multiple pieces) of the ankle joint. High energy impacts, such as motor vehicle collisions and falls, are common causes of pilon fractures, which comprise approximately 5-10% of all tibia fractures (Wei, Han, Lan, & Cai, 2014). At the time of injury and throughout recovery, deep infection, mal-union and non-union are common complications (Viberg, Kleven, Hamborg-Petersen, & Skov, 2016). In the general population, ankle osteoarthritis (OA) is uncommon. However, following fractures or severe ankle sprains, approximately 70% of patients develop ankle OA (Cushnaghan & Dieppe, 1991; Saltzman et al., 2005). Overall, decreased functional outcomes and quality of life have been observed in pilon fracture patients when compared to a healthy population (De-las-Heras-Romero et al. 2017).

Pilon fractures remain difficult to treat due to the complexity of the fracture and the associated soft tissue damage (Wei et al., 2014). Two surgical treatment options are available for pilon fractures: anterolateral and medial fixation plates. These plates aim to stabilize the fracture site while providing optimal conditions for bone healing to occur. However, the biomechanical characteristics of these plates are poorly understood (Pirolo, Behn, Abrams, & Bishop, 2015). Previous studies have used the construct stiffness to evaluate the differences between the two plates, but none have examined a true pilon fracture in a cadaveric model with fibular involvement

[1] Anatomical terms used in document are listed in APPENDIX A: Glossary of Medical Terms

(Pirolo et al., 2015; Yenna et al., 2011). It is important to consider the entire tibiofibular syndesmosis as the fibula is a load bearing component and is often fractured as well in a pilon fracture (Barei, Nork, Bellabarba, & Sangeorzan, 2006). A more detailed investigation of these plates is needed to relate the choice of plate to effectiveness at promoting bone healing.

The goal of this research was to determine the effectiveness of the anterolateral and medial fracture fixations by comparing the construct stiffness, strength and motion of the bone fragments under the immediate post-surgical condition using cadaveric specimens. An improved understanding of how these plates function to heal pilon fractures will help guide surgeons in treating these severe injuries, thus reducing patient complications and increasing functional outcomes.

1.2 Bones

1.2.1 Anatomy

The long bones of the lower leg consist of the tibia and the fibula (Figure 1.1). The proximal end of the tibia connects to the upper leg via the knee joint. The tibia runs along the middle of the leg and is the larger, primary weight-bearing bone of the lower leg. The fibula is parallel to the tibia on the lateral side, and is connected by the interosseous membrane. The fibula bears approximately 10-15% of the total axial compressive load in the leg and its primary purpose is for muscle attachments (Kuppa, Wang, Haffner, & Eppinger, 2008). Long bones, such as the tibia and fibula, are described as having two sections: epiphysis, and diaphysis (Figure 1.2), each with anisotropic properties. The epiphysis is primarily composed of the structural unit trabeculae (trabecular bone) and its orientation determines the anisotropy (Doblaré, García, & Gómez, 2004).

The diaphysis is composed of compact bone, which is comprised of osteons that run in the longitudinal direction. Within an osteon there are concentric layers of lamellae that surround the Haversian canal (space for the nerves and blood vessels). Volkmann's canals are found within the osteon and connect the Haverisan canal. The orientation of the lamellae and osteons determines the anisotropy (Doblaré et al., 2004).

The interosseous membrane, the anteroinferior tibiofibular ligament, and the transverse tibiofibular ligament are the most notable structures that form the tibiofibular syndesmosis (Figure 1.3). The distal end of the tibia and the fibula form a concave surface that articulates with the talus, also known as the tibial plafond. The tibia, fibula and the talus are the three bones that comprise the tibiotalar (ankle) joint. The ankle joint contributes to the ability to walk through plantar and dorsiflexion of the foot.

1.2.2 Bone Healing

During a fracture, the continuity of the bone is disrupted. To successfully heal the bone, an adequate blood supply and biomechanical stability are required (Marsell & Einhorn, 2011). The mechanical stability at the fracture site determines the type of bone healing that will occur, where primary and secondary bone healing are the two processes that both result in a bone structure similar to that before the injury (Doblaré et al., 2004; Sfeir, Ho, Doll, Azari, & Hollinger, 2005).

Primary bone healing can take two forms: gap healing and contact healing. Bone union is achieved through both of these processes without the formation of a bony callus. Below is a description of the processes, summarized from Sfeir et al. (2005).

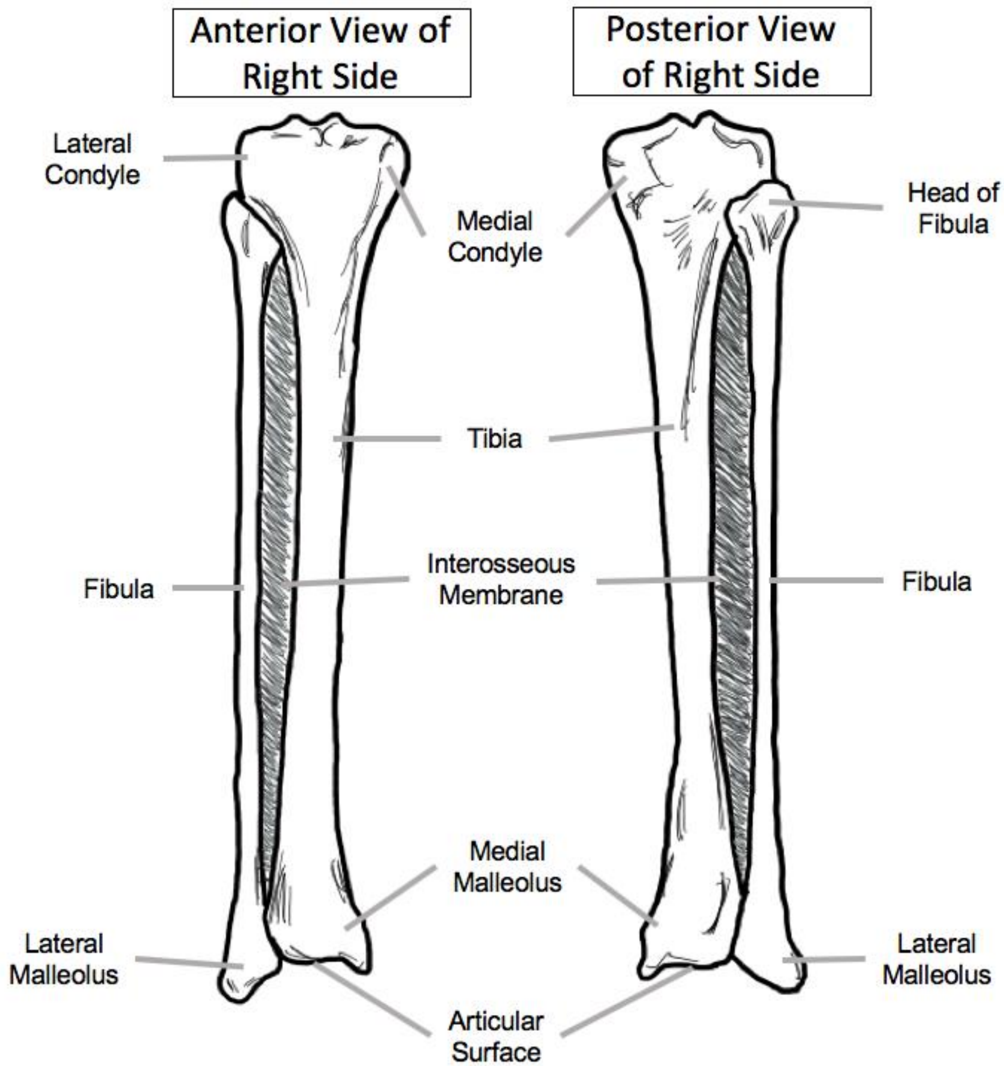

Figure 1.1: The Anatomy of the Tibia and the Fibula.
The lower leg is made up of two primary bones, the tibia and the fibula. Between the two is the interosseous membrane, a stiff tissue that facilitates load sharing between the bones.

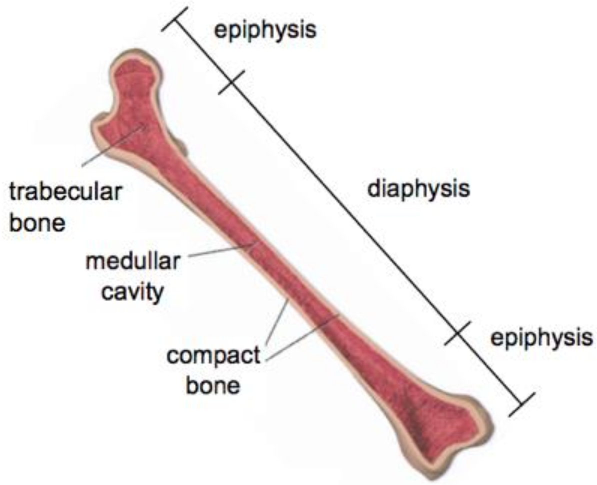

Figure 1.2: Structure of a Long Bone.
A typical long bone consists of two sections: epiphysis and diaphysis. The epiphysis is formed primarily of trabecular bone, and carries load from the joint to the diaphysis, which is made from compact bone. Photo modified from Piccinini (2014).

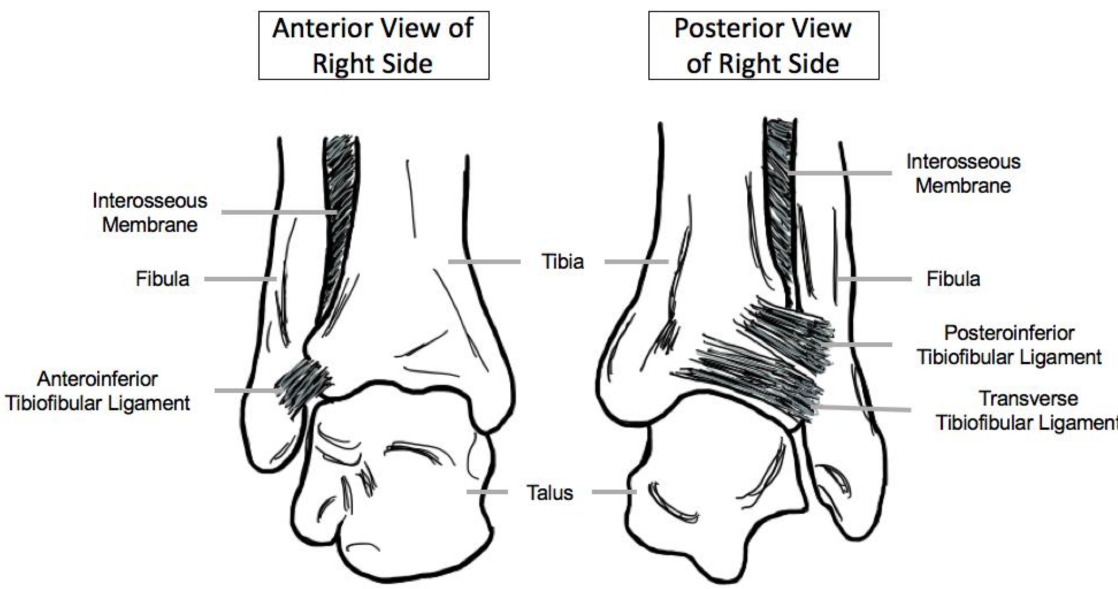

Figure 1.3: Anatomy of the Ankle Joint.
The four main structures that connect the distal tibia to the fibula are the interosseous membrane, the anteroinferior tibiofibular ligament, the posteroinferior tibiofibular ligament and the transverse tibiofibular ligament. These structures make up the tibia fibula syndesmosis.

Gap healing occurs when there is a gap of 0.8 mm - 1 mm between the bone fragments (Marsell & Einhorn, 2011). Firstly, a scaffold of bone is laid down perpendicular to the long axis of the bone. Secondly, the necrotic fracture ends are reconstructed by longitudinal Haversian remodeling, thus replacing the fractured bone with osteons of the original orientation. This leads to the final bone structure, similar to the architecture before the injury.

Contact bone healing occurs when the bone fragments are in contact with each other. Osteons grow across the fracture site, parallel to the long axis of the bone. On one side of the fracture site, cutting cones cross the fracture lines via a tunneling resorptive response. The cavity allows penetration of the capillary, establishing a new Haversian system. These blood vessels contain endothelial cells and osteoblasts that allow for the production of osteons across the fracture line. Normal bone structure is then achieved.

Secondary bone healing (indirect bone healing) is the most common form of bone healing, and weight bearing and appropriate levels of micromotion enhance the process. Secondary bone healing consists of four phases: inflammation, soft callus formation, hard callus formation and remodeling. This is a continuous process that starts immediately at the time of injury and can last up to several years.

Inflammation occurs after the fracture occurs, signifying soft tissue damage and the separation of bony fragments. A hematoma is formed, which consists of cells to resorb the necrotic bone tissue and begin the healing process. This process peaks 24 hours after injury and can last up to seven days. Mesenchymal stem cells, found in the hematoma, begin to form chondroblasts, fibroblasts and osteoblasts. The fibroblasts attract fibrin to initiate the formation of the soft callus forming fibrin rich tissue. With the stimulation of motion between the bone fragments, the fibrin is then woven together to form the soft callus. The soft callus, filled with fibrous connective tissue, blood vessels, cartilage, and woven bone, is then calcified to form the hard callus, providing biomechanical stability. Remodeling then occurs under the influence of mechanical loading until complete stability is achieved. The osteoclasts continue to remove bone and the osteoblasts will lay bone weeks after the fracture, spanning over the entire lifetime. The fracture healing process is completed when there is restoration of the intramedullary canal and the architecture of the bone is similar to the bone prior to the fracture.

1.2.3 Fracture Treatment

The strain at the fracture site controls the type of healing that occurs at the fracture site. The strain is determined by the mechanical stability (Hak, Toker, Yi, & Toreson, 2010). Strain, from a biomechanical perspective, is defined by Egol *et al*. (2004) as the "*relative change in fracture gap divided by the fracture gap*." The optimal strain for fracture healing to occur ranges from 2-10%. With too much motion between the bone fragments (*i.e.,* strain > 10%), the soft callus will not be able to transition to the hard callus causing non-union or mal-union. In contrast, too little motion will not stimulate the formation of any callus; therefore, no healing will occur. Thus, the bone fragments must be reduced properly and receive the appropriate amount of support for proper bone healing to occur. Mechanical stability is provided at the fracture site through the use of orthopedic devices. These devices control the motion of the bone fragments and either provide absolute or relative stability, where "absolute" stability is defined as "*anatomic reduction and interfragmentary compression with absence of fracture micromotion under physiologic load*" (Kojima & Pires, 2017).

Rigid fixation will provide absolute stability, by providing compression to the fracture to limit the amount of motion of the bone fragments to a strain less than 2%, resulting in primary bone healing (described in Section 1.2.2). Lag screws and compression plates are two methods that provide compression at the fracture site (Figure 1.4) (Norris et al., 2018).

Relative stability is achieved through the use of casts, intramedullary (IM) nails, locked plates and external fixators. These fixations allow the strain between bone fragments to range from 2-10%, which stimulates secondary bone healing (described in Section 1.2.2). A cast is a shell placed around the injured limb to immobilize the site of the fracture and is removed once the bone is sufficiently healed. It is commonly used to treat a simple break of the bone. Intramedullary (IM) nails are often used to treat extra-articular tibial fractures. The IM nail is inserted through the intramedullary canal in order to support the fragments of bone during healing. Intermedullary nails have been shown to cause increased cases of mal-alignment when compared to tibial plating (Vallier, Cureton, & Patterson, 2011). Locked plates are connected to the bone through screws and create a gap between the bone and plate; the screw heads are "locked" into the plate through threading, which allows stability with this offset. This is beneficial as it does not cause damage to the periosteum or inhibit the blood supply (Figure 1.5).

An external fixation may be used as a temporary fixation while the soft tissues heal enough before performing surgery; however, it does not provide direct visualization to the articular surface (Bear, Rollick, Helfet, & Bear, 2018).

Relative stability and secondary bone healing are thought to be the goals of fixation techniques as they work to decrease the strain by minimizing motion and tolerating increased gap length (Egol, Kubiak, Fulkerson, Kummer, & Koval, 2004).

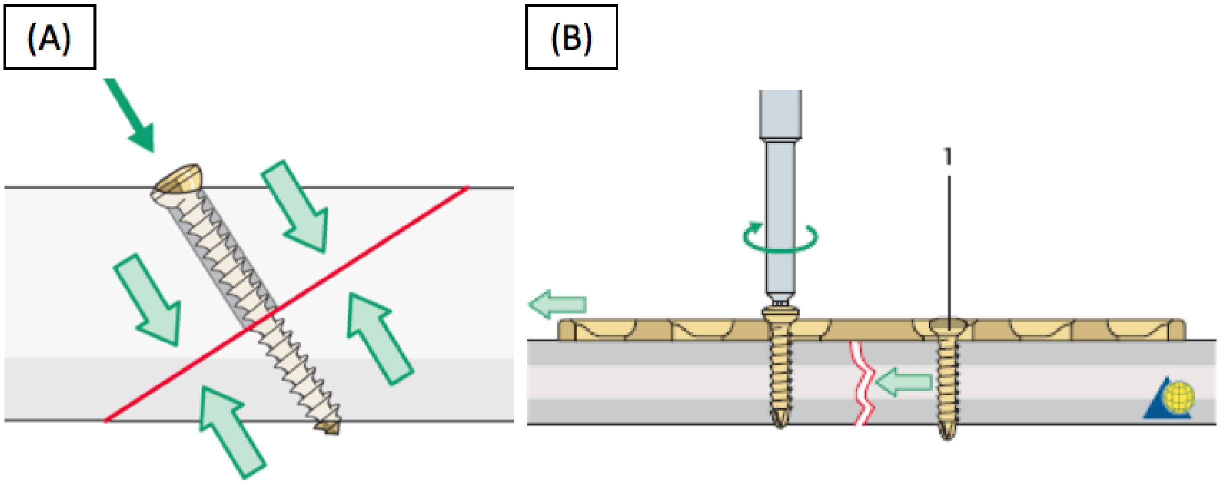

Figure 1.4: Types of Fixations Resulting in Compression.
(A) A lag screw is used to join provide interfragmentary compression to the bone fragments to limit the amount of motion at the fracture site (White & Camuso, 2012). (B) Compression plating is achieved by tightening the screw in order to shift the plate and move the bone fragments to compress the fracture (Ruedi, Buckley, & Moran, 2007)

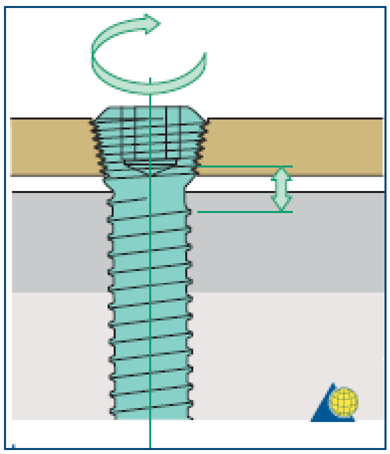

Figure 1.5: Mechanism for Locking Plates.
Locking plates and screws are used to keep the plate away from the bone such that the periosteum and the blood supply are not affected. “Locking” is achieved by threading on the screw head providing stability as the plate is offset (Ruedi et al., 2007).

1.3 Pilon Fractures

1.3.1 Mechanism

A pilon fracture occurs under a large axial compressive load that applies a high amount of energy to the distal tibia and represents 5-7% of all tibial fractures (Figure 1.6(A)) (Bonar & Marsh, 1994; Mauffrey et al., 2011). Common causes of pilon fractures are motor vehicle collisions and falling from a height (Bonar & Marsh, 1994). During these traumatic events, the talus is driven up through the articular surface of the tibial plafond, distributing the force over the distal end of the tibia and fibula causing multiple fractures (Sitnik, Beletsky, & Schelkun, 2017). Typically, this results in three tibial fragments: anterolateral, posterolateral and medial (Figure 1.6(B)) (Jacob et al., 2015). Pilon fractures often cause soft tissue damage and are characterized by bone comminution and articular surface disruption (Bonar & Marsh, 1994).

1.3.2 Classification

Distal tibia fractures are described by the Müller AO Classification of Fractures (Figure 1.7), and are classified based upon "*the degree of articular involvement and comminution and impaction in the metaphysis and epiphysis*" (Müller, 1987; Wei et al., 2014). Type 43-C is a pilon fracture due to the level of comminution and articular involvement to the distal tibia, with 43-C3 having the most articular surface involvement and bone fragments. Type 43-C3 is the focus of this thesis.

In addition to this fracture classification, pilon fractures can be further described as varus or valgus based on the orientation of the wedge, with varus having a medially-opening wedge and valgus having a laterally-opening wedge (Figure 1.8).

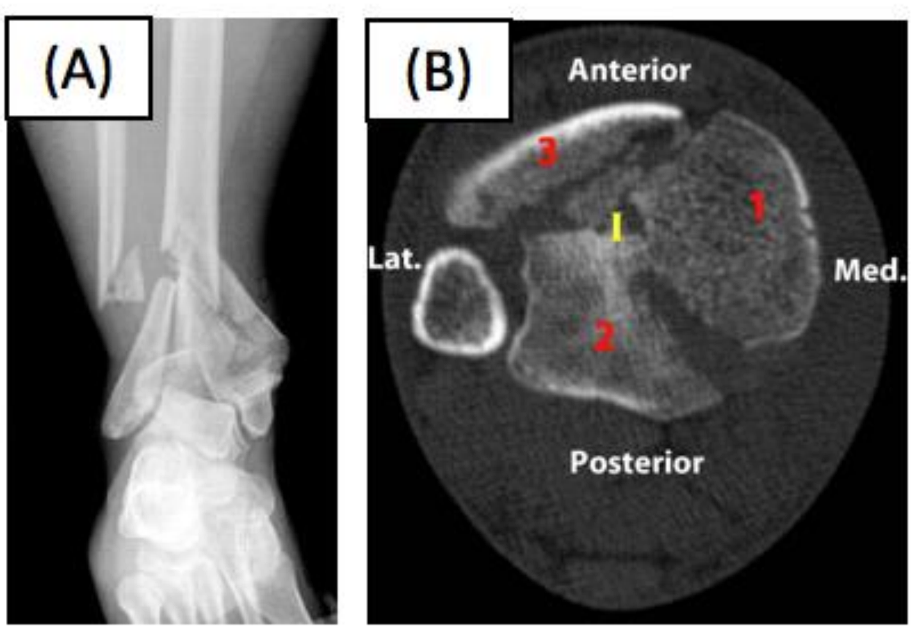

Figure 1.6: Radiographs of a Pilon Fracture.
(A) Frontal view of a pilon fracture (comminution to the ankle and a fibular fracture). A pilon fracture may occur when there is a high compressive load to the ankle joint (Crist, Khazzam, Murtha, & Rocca, 2011). (B) Axial view of a CT scan of a Pilon Fracture showing the common location of bone fragments resulting from a pilon fracture (1) anteromedial (2) posterior (3) anterolateral (Cole, Mehrle, Bhandari, & Zlowodzki, 2013).

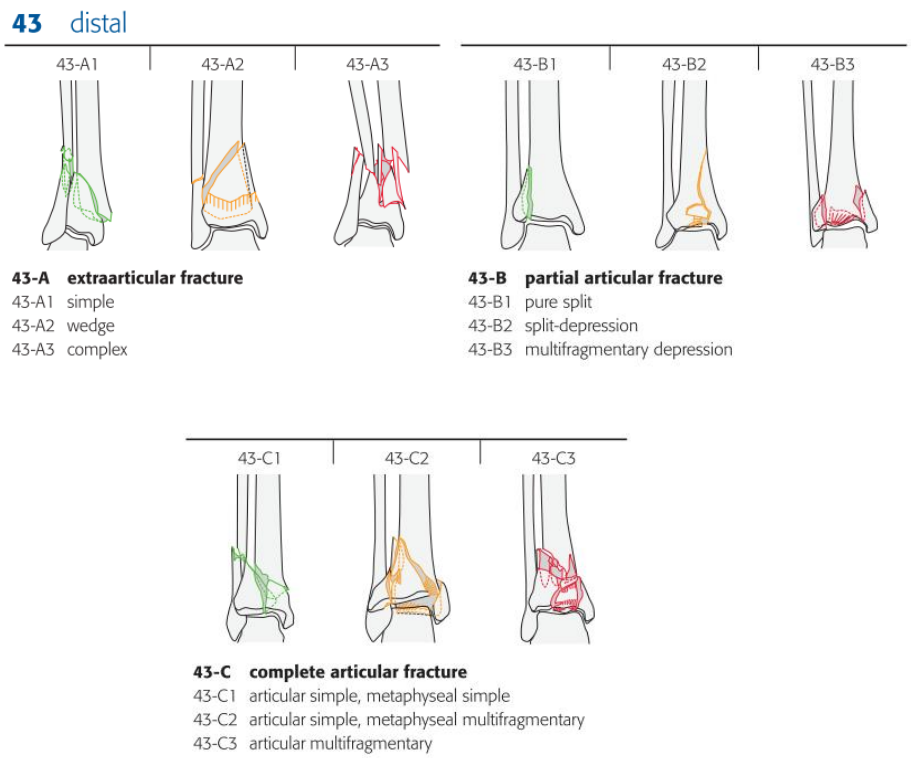

Figure 1.7: Fracture Classification of the Distal Tibia.
43-C3 distal tibial fractures were the focus of this thesis as they have the most articular involvement and bone fragments (Müller, 1987).

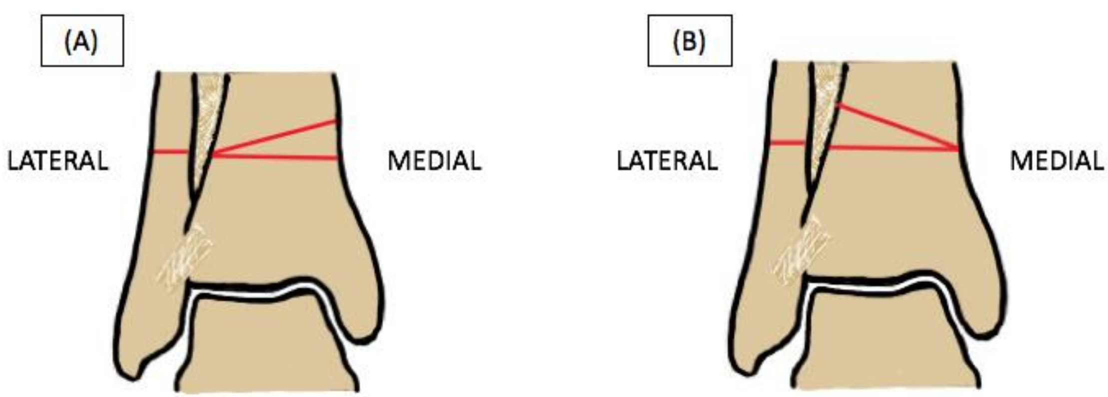

Figure 1.8: Pilon Fracture Pattern Classification.
(A) Varus fracture pattern shown on a right tibia fibula syndesmosis (wedge opening to the medial side); and (B) Valgus fracture pattern shown on a right tibia fibula syndesmosis (wedge opening to the lateral side).

1.3.3 Treatment

Pilon fractures are commonly diagnosed with an x-ray image in order to determine the fracture pattern, providing important information for planning treatment (Jacob et al., 2015). The mainstay treatment option for pilon fractures is open reduction and internal fixation (ORIF), where an orthopedic surgeon exposes the fracture site, reduces the fracture and implants a fracture fixation device to stabilize the fracture (Sitnik et al., 2017). Jacob et al. described how "*successful treatment of pilon fractures is dependent on the management of soft tissue injury, anatomical reduction in the joint surface and restoration of mechanical alignment*" (Jacob et al., 2015). Therefore, the aims of surgical treatment as defined by Sitnik et al. (2017) are:

- *anatomical restoration of the joint surface with correct axial alignment;*
- *stable internal fixation to allow for early functional treatment; and*
- *careful, atraumatic surgical technique to preserve blood supply to the bone and soft tissue.*

To achieve these goals, locking compression plates are used to treat tibial fractures as previously described in Section 1.2.3. There are two styles of plates that are currently used to treat pilon fractures: anterolateral and medial plates (named based on the location where they are applied) (Figure 1.9). These plates bridge the fracture site and allow relative stability (strain 2-10%) by providing compression at the fracture site while minimizing disruption to the periosteum and the blood supply.

Table 1.1 provides an overview of the benefits and difficulties associated with the use of anterolateral plates and medial plates.

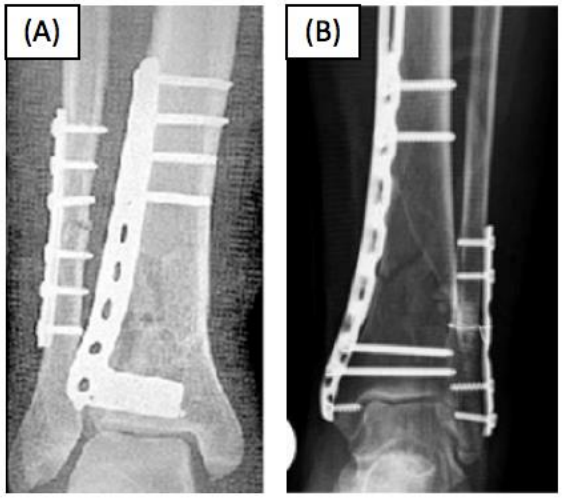

Figure 1.9: Plates Used to Treat Pilon Fractures.
(A) Distal tibia and fibula fractures treated with anterolateral (Garg et al., 2017) and (B) medial plates (Kim & Chung, 2014). Note the fibula is repaired in each with a standard plate.

Table 1.1: Comparison of Anterolateral and Medial Plates.
Anterolateral and medial plates have both been shown to have benefits and challenges.

	Anterolateral Plate	**Medial Plate**
Benefits	• Shown to have mechanical benefits in patients with distal tibia fractures with valgus fracture pattern (Casstevens et al., 2012) • More soft tissue coverage (Grose et al., 2007; Manninen, Lindahl, Kankare, & Hirvensalo, 2007)	• Good exposure to the tibia (Garg et al., 2017) • Decreased local soft tissue damage (Pirolo et al., 2015)
Difficulties	• Does not capture all fracture lines (Aneja et al., 2018) • More dissection is needed near important neurovascular structures therefore increased risk of damage (Teeny & Wiss, 1993; Wolinsky & Lee, 2008) • Arteries at risk: dorsalis pedis and deep peroneal & terminal branches of the peroneal nerve (Wolinsky & Lee, 2008)	• Comments from Garg et al. (2017): o High risk of wound infection o Second incision is needed if fibula fixation is necessary o Hardware discomfort o Increases skin tension o Disruption of the blood supply

1.3.4 Fragment Motion

As previously mentioned, a strain of 2-10% is required for secondary bone healing to occur. Therefore, the strain may be determined by evaluating the micromotion of the bone fragments during loading. A previous study (Muizelaar, 2012) utilized a 3D motion tracking system to determine the amount of strain of a periprosthetic fracture gap.

Motion tracking system are advantageous as they are non-contact, have a high sampling frequency and allow freedom for tracking movement. The system uses infrared cameras to track the displacement of reflective markers that are placed on points of interest. Muizelaar (2012) recommended refining the system to optimize the accuracy. This includes adjusting the position of the cameras and the markers to ensure the markers are visible at all times during the trial. Optical tracking has yet to be used to assess the interfragmentary motions for pilon fractures.

1.4 Background

Although there are clear benefits and challenges associated with both the anterolateral and medial plates, there has been no conclusion, from a biomechanical perspective, as to which plates should be used to treat a varus or valgus fracture type. Currently, the choice of pilon fracture treatment is based upon the fracture pattern, the severity of the soft tissue injury, and the treating surgeon’s experience (Jacob et al., 2015).

Two previous studies have recommended that medial plates should be used for varus fractures. Pirolo et al. (2015) previously investigated the use of these plates in a synthetic tibia bone model with a simple (non-comminuted) fracture pattern. This study found that the medial plating showed a superior level of stiffness when compared to the anterolateral plate. Similarly, Yenna et al. (2011) also compared the use of these plates using a synthetic tibia bone model in addition to an extra-articular fracture pattern. They also concluded that the medial plate provided greater stiffness when compared to the anterolateral plate. Both studies modeled an extra-articular fracture pattern and in order for it to be considered a pilon fracture, articular involvement is necessary. Furthermore, the use of synthetic bones limits the generalizability of their findings and lacks the presence of the fibula, which is important to consider as the fibula is often fractured as well (Barei et al., 2006).

The treatment of the fibula is often debated. Bear et al. (2018) showed that fixation of the fibula is necessary to stabilize the syndesmosis and assists in the reduction of the plafond. Casstevens et al. (2012) suggested that it indirectly stabilizes the tibia by stabilizing the syndesmosis, but should be avoided if it obstructs the reduction of the tibia (Casstevens, Le, Archdeacon, & Wyrick, 2012). Conversely, non-union of the tibia has been shown to be more common when there is fixation of the fibula (Vallier, Le, & Bedi, 2008).

To date, there are no known studies that have examined true pilon fractures in a cadaveric model to assess the biomechanical performance of these two common plating options.

1.5 Study Rationale and Overview

1.5.1 Rationale

In light of the continued challenges associated with these plates, high incidence of OA, and lack of biomechanical studies that examine the realistic fracture condition using a tibia fibula syndesmosis, a new biomechanical study was needed that evaluated the performance of the plate used for treating a varus fracture pattern. The techniques developed herein could be applied in the future to a valgus fracture pattern.

1.5.2 Objectives

The objectives of this thesis were:

1. To compare the stiffness (N/mm) and strength (N) of the medial and anterolateral plated specimens when used to treat a varus type pilon fracture.
2. To develop a novel application for the motion tracking system to estimate the overall motion of the bone fragments during loading to evaluate the stability the plates would provide under post-operative loading conditions.

The hypothesis for this study was:

- The medial plate would perform show superior performance results (*i.e.* a greater stiffness and strength and reduced overall fragment motion) for a varus fracture pattern.

1.5.3 Thesis Overview

This thesis continues to present how the objectives of this thesis were achieved in the following order:

- Chapter 2 of this thesis provides the assessment from a stiffness and strength perspective.
- Chapter 3 outlines the development of techniques used to determine the overall motion of the bone fragments.
- Chapter 4 provides the discussions and conclusions for the entire thesis, including the clinical implications of the present work.

Chapter 2: Evaluation of the Construct Stiffness and Strength of Repaired Specimens

2.1 Introduction

Pilon fractures comprise 5-7% of all tibial fractures and are characterized by comminution at the ankle joint (Bonar and Marsh 1994; Mauffrey et al. 2011; Korkmaz et al. 2013). Currently, the mainstay treatment for pilon fractures is open reduction and internal fixation, which allows for excellent visualization for reducing the fracture. During this procedure, the fracture is typically treated with either an anterolateral or medial plate and the current approach for plate selection is to place the plate on the opening side of the wedge fracture; hence, medial plate for a varus type fracture and anterolateral for a valgus type fracture. However, patients still report negative outcomes affecting their quality of life, regardless of treatment method (Cutillas-Ybarra, Lizaur-Utrilla, and Lopez-Prats 2015).

The relative performance of these two plating types has been previously investigated and unclear conclusions have been reported. One study (Pirolo et al., 2015) compared the construct stiffness of the anterolateral and medial plate for varus and valgus extra-articular fracture patterns. They modeled these fracture types on synthetic composite bones and found that medial plating provided higher stiffness for a varus fracture type. Similarly, another study (Yenna et al., 2011), compared the construct stiffness for a varus and valgus distal tibia extra-articular fracture pattern when treated with an anterolateral and medial plate using synthetic composite bones. In this study, they loaded the specimens in a medial and posterior position. They found that the medial plate was stiffer than the anterolateral plate when loaded in the medial position with the wedge removed.

This difference was found to be statistically significant; however, the difference was not statistically significant when loaded in the posterior position.

Given the unclear results, lack of a fibula, use of synthetic bones and a simple (non-comminuted, extra-articular) fracture pattern, there remains a need to investigate the plating performance for pilon fractures. The purpose of the present study was to evaluate the stiffness and strength of anterolateral and medial plates when used to repair comminuted intra-articular pilon fractures using a cadaveric tibia and fibula syndesmosis.

2.2 Methods

2.2.1 Specimen Preparation

Eight pairs of lower leg cadaveric specimens (mean age 77±8 years, three male and five female) (Table 2.1) were used for this study. The left and right pairs were randomly allocated in two groups (medial and anterolateral plated) to allow for a direct comparison between the anterolateral and medial plates. The specimens were dissected to isolate the tibia and fibula while maintaining the integrity of the interosseous ligament, anterior inferior tibiofibular ligament, posteroinferior tibiofibular ligament and transverse tibiofibular ligament (Figure 1.3). The specimens were then potted proximally in a 4x4x2.5” square tube using dental cement (Denstone Golden, Heraeus Kulzer, South Bend, IN, USA) to secure it in an inverted position (ankle end up). To consistently align the specimens, a bull’s eye level was placed in the articular surface of the tibial plafond to align it in the frontal and sagittal planes, and the tibial plateau was centered within the tubing (Figure 2.1). The bull’s eye level was raised on a coupler to accommodate the various depths of the articular surface. Specimens were thawed for four to six hours prior to any testing.

Table 2.1: Specimen Information.
Information for the specimen pairs used for this study. Specimen pairs 1-6 were used for the intact testing while specimen pairs 3-8 were used for the plating portion of this study.

Specimen Pair	Age (years)	Sex	Plating Method	
			Left	Right
1	82	Female	-	-
2	74	Male	-	-
3	61	Female	Medial	Anterolateral
4	87	Female	Anterolateral	Medial
5	78	Male	Medial	Anterolateral
6	84	Female	Medial	Anterolateral
7	84	Male	Anterolateral	Medial
8	72	Female	Anterolateral	Medial

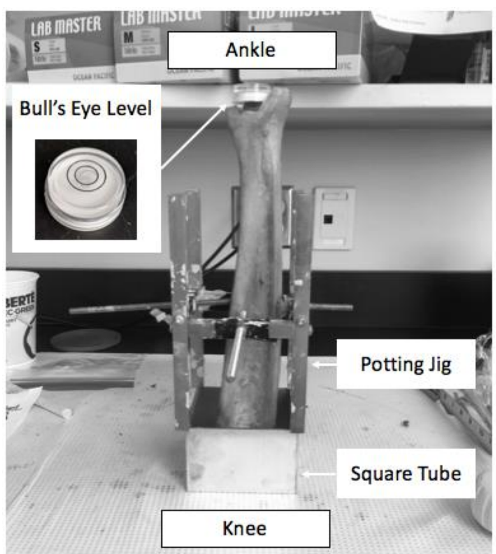

Figure 2.1: Specimen Set-Up During the Potting Process.
Each specimen was placed with the proximal end in a square tube and aligned using a bull's eye level. The potting jig maintained the alignment while dental cement was poured in the square tube to secure it.

2.2.2 Intact Stiffness Testing

Specimen pairs 1-6 (Table 2.1) were used for the intact specimen testing as specimen pairs 7-8 were already fractured and repaired. Specimen pairs 1 and 2 were allocated to another study investigating valgus type pilon fracture patterns; therefore, specimen pairs 3-8 were used for the plating portion of the study. This resulted in an N = 6 for each phase of the test. As the mating talus was not available, an artificial one was made for each specimen by creating a mold of the articular surface from dental cement to match the natural geometry and have even load distribution (Figure 2.2).

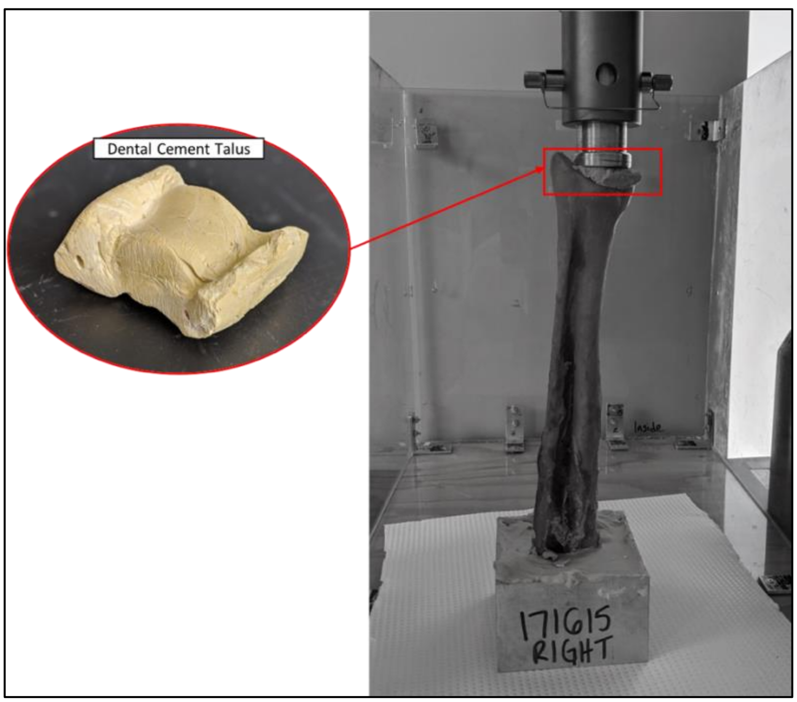

Figure 2.2: Detail View of the Dental Cement Talus.
A specimen loaded in the materials testing machine with a detail view of the dental cement talus. While creating the dental cement talus, plastic wrap was used to contain the cement within the articular surface, to ensure it was the only area that would be loaded.

Using a materials testing machine (Instron 5967, Norwood, MA, USA) cyclic loads were applied quasi-statically at a rate of 0.1 mm/s for 10 cycles for each of the following ranges of load: 10-50 N, 10-100 N, 75-400 N, 100-700 N, 100-1000 N and 100-1400 N, which were selected based on similar studies (Pirolo et al., 2015) and the estimated post-operative loading (Tschegg et al., 2008) (Figure 2.3). The load (N) and deformation (mm) were outputted from the material testing machine and the load was divided by the deformation to determine the construct stiffness (N/mm). The specimens that were allocated to the anterolateral group were compared to the medial plated specimens using a paired t-test (α=0.05).

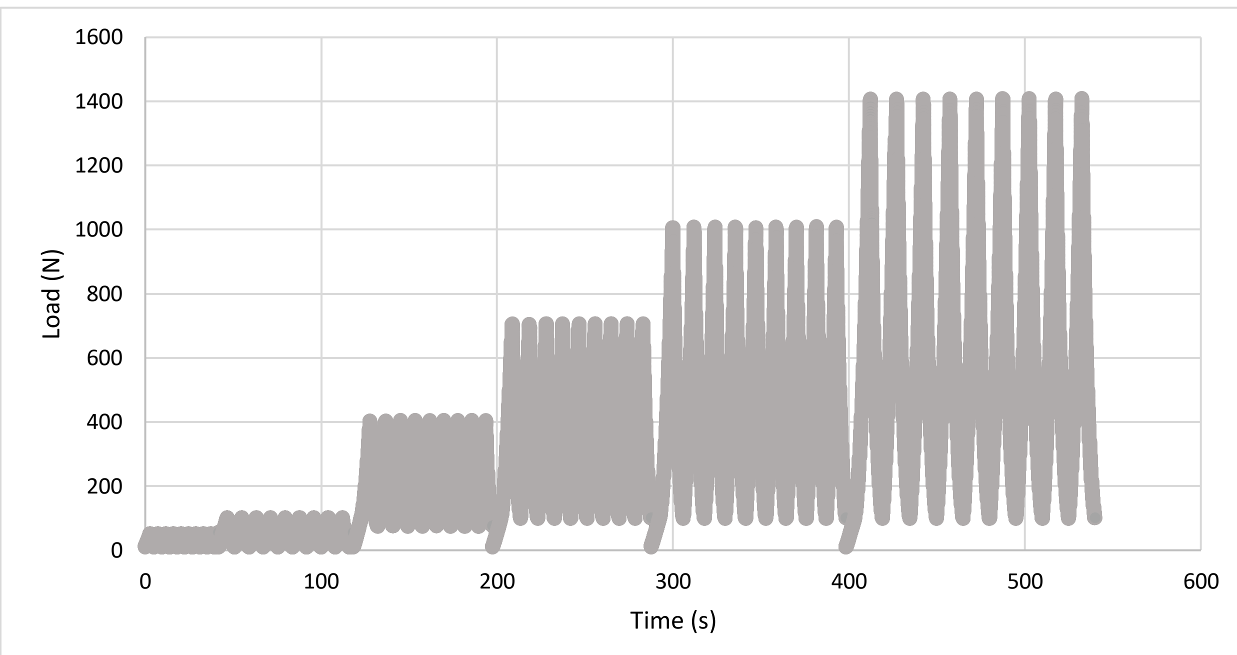

Figure 2.3: Sample Graph of Cyclic Loading Sequences for Specimen 2 (left).
Ten cycles were tested at each of the following loading ranges: 10-50 N, 10-100 N, 75-400 N, 100-700 N, 100-1000 N and 100-1400 N.

2.2.3 Fracturing and Plating[2]

To remove the variability associated with surgical reconstruction and to ensure consistent fracture gaps, plates were applied prior to creating the fracture. The required tibial plate and tubular plate (for the fibula) (Depuy Synthes, Markham, ON) were fitted onto the bone and then the holes were pre-drilled and tapped before inserting the screws (Depuy Synthes, Markham, ON). The plates were then removed to create a gap. The fracture pattern used was developed by the collaborating orthopaedic surgeon. A Y-type intra-articular fracture was marked on the articular surface with a template (Figure 2.4 (A)). A varus wedge fracture was created by marking 4 cm from the medial gutter (lowest point on the anteromedial surface of the tibia) and measuring 1 cm proximally to create the varus wedge fracture (Figure 2.4 (B), Figure 2.4 (C)). A transverse fibular fracture was created aligned with the vertex of the wedge fracture. The fractures were created using an oscillating saw (blade thickness 0.58 mm, Dremmel Multi-Max, Wood Flush Cut Blade MM470, Mount Prospect, IL). The plates were then screwed onto the specimen while lining them up with the pre-drilled holes.

[2] Specification for the Hardware are in APPENDIX B: Hardware Information

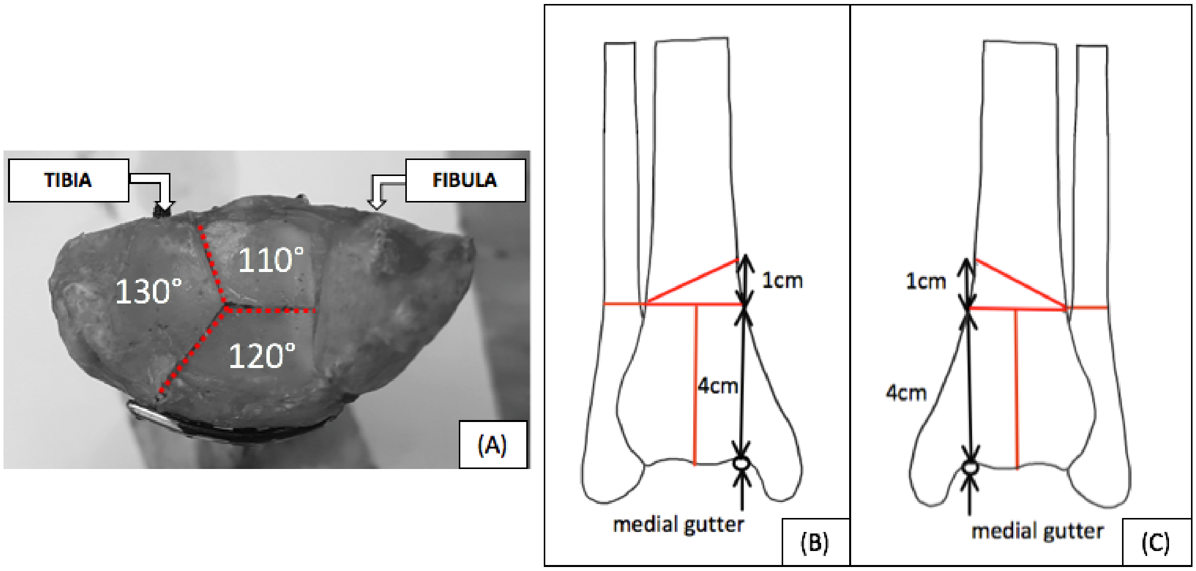

Figure 2.4: Fracture Pattern Created on the Specimens.
(A) Transverse view of the tibia and fibula showing a Y-type coronal fracture pattern for the articular surface of all specimens that extended up the long axis of the tibia. (B) Anterior view of the tibia and fibula pattern for right specimen. (C) Anterior view of the tibia and fibula fracture pattern for a left specimen.

2.2.4 Mechanical Testing

After fracturing, there was a slight narrowing of the articular surface, therefore a new talus mold (Denstone Golden, Heraeus Kulzer, South Bend, IN, USA) was created. To ensure no penetration of the fracture gaps, the articular surface was lined with plastic wrap.

Due to the reduced strength of the repaired specimen, there was a greater amount of deformation when compared to the intact specimens. Therefore, the load levels were decreased based upon the similar amount of deformation observed at 1400 N for the intact specimens. The specimens were then loaded up to 400N according to the protocol in Section 2.2.2 (Figure 2.4).

The construct stiffness was calculated for each specimen based on the average of the last three cycles and compared between plating groups using a paired t-test (α=0.05).

The dental cement talus mold did not withstand the loads to undergo failure testing, therefore, a new bone cement talus was created for each specimen (Polymethylmethacrylate, Surgical Simplex, Stryker, Canada), using the same method as the dental cement talus. Specimen pairs 3-6 were then loaded a rate of 0.1 mm/s until failure, which was defined as a load drop greater than 100 N. The peak loads were compared using a paired t-test (α=0.05).

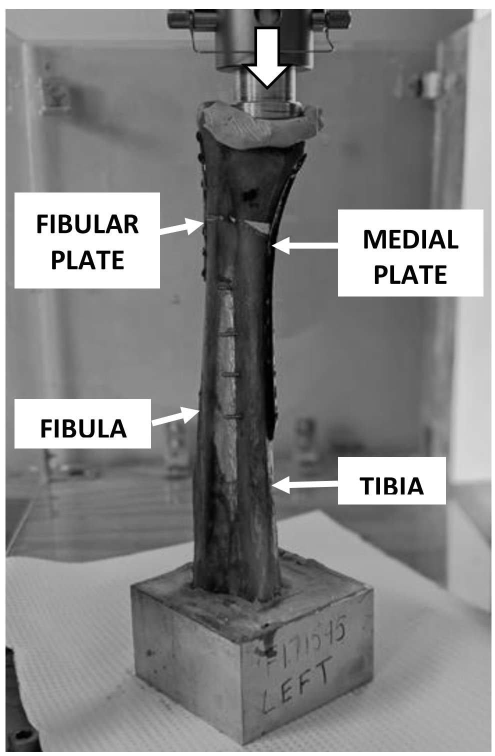

Figure 2.5: Specimen Set-up in the Materials Testing Machine.
Medial plated specimen set up in the materials testing machine. The top arrow represents where the load was applied during testing.

2.3 Results

2.3.1 Intact Specimen Testing[3]

The amount of deformation experienced by the intact specimens increased with an increasing amount of load (Figure 2.6). After 100 N, there was an increase in the amount of deformation. The stiffness also increased with an increase in load (Figure 2.7). When comparing the groupings for the two treatment methods, there were no significant differences found (p=0.99), therefore the pairs were considered equivalent.

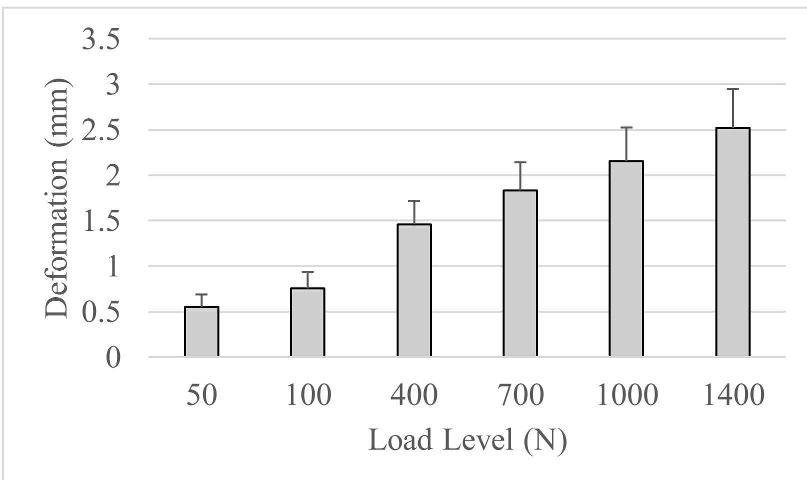

Figure 2.6: Deformation Results for the Intact Specimens.
The resulting amount of deformation for the specified load levels for intact specimens. Specimen pairs 1-6 (Table 2.1) were used to find the resulting amount of deformation at intermittent load levels (N=12).

[3] Stiffness values from this section are in APPENDIX C: Tabulated Data for Intact Specimen Testing

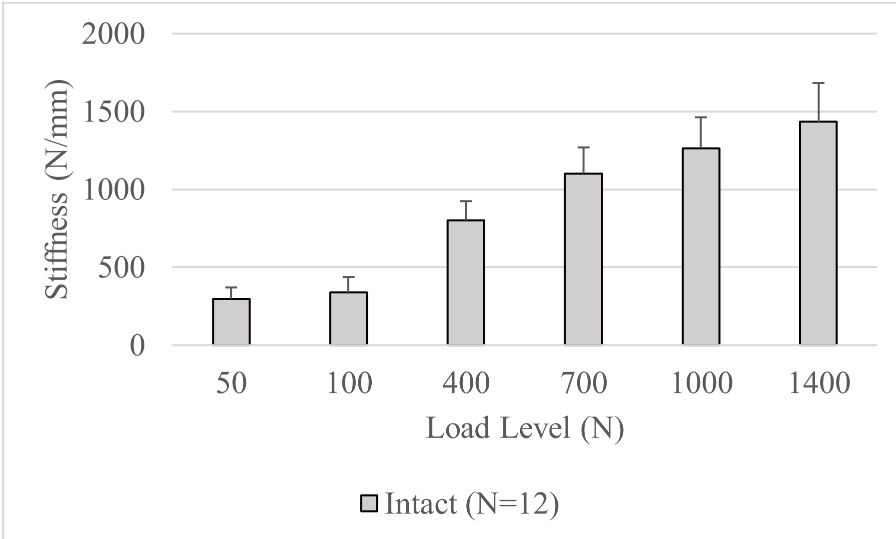

Figure 2.7: Stiffness Results for the Intact Specimens.
Stiffness was found by calculating the slope of the force displacement curve for the last three cycles of the test (N=12).

2.3.2 Repaired Specimens

Due to the comminution, the repaired group was likely to sustain more deformation, therefore the repaired group was not loaded to the same level as the intact group. The amount of load applied to the repaired specimens was selected by finding the load that corresponded to similar amounts of deformation as the intact specimens (2.5 mm for 1400 N load). The mean deformation for the repaired specimens at 400 N was 2.4 mm (Figure 2.8), and thus was used for stiffness testing.

The medial plated specimens tended to be stiffer than the anterolateral plated specimens (601.7 ± 135.2 N/mm and 473.6 ± 150.3 N/mm, respectively), but this was not statistically significant (p=0.28) (Figure 2.9).

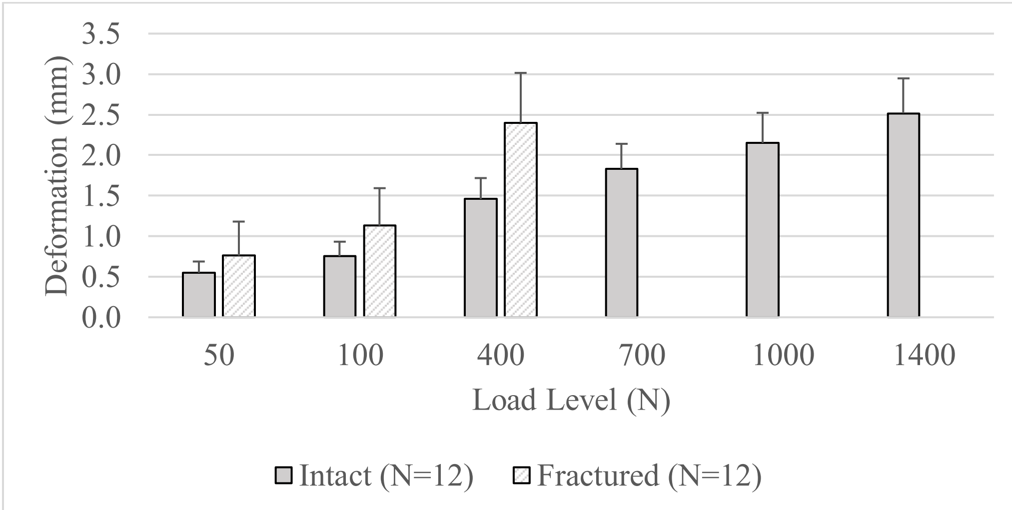

Figure 2.8: Amount of Deformation that Occurred at the Various Loading Ranges.
Results showing the amount of deformation (mm) occurring at different loading levels for the intact specimens. Intact testing was conducted on Specimen pairs 1-6 and repaired testing was conducted on Specimen pairs 3-8 (Table 2.1).

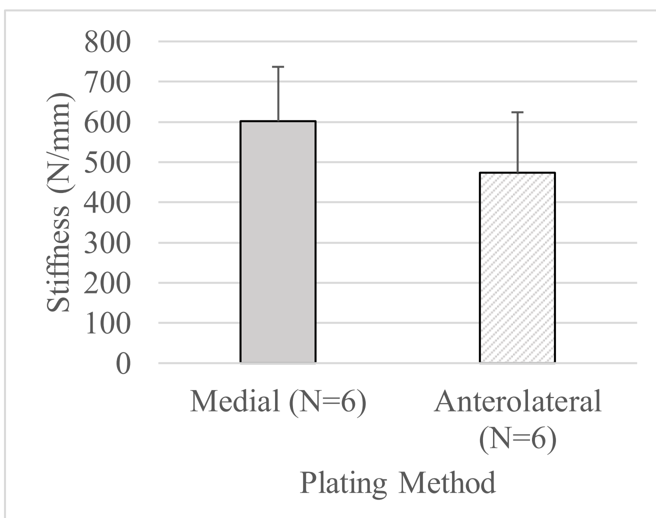

Figure 2.9: Stiffness Results for Repaired Specimens.
Comparison of the stiffness for the medial and anterolateral plated groups ($p = 0.28$) (Specimen pairs 3-8 from Table 2.1).

2.3.3 Failure Testing

The medial plated specimens failed at a load of 3096.1 ± 1825.7 N, while the anterolateral specimens failed at a load of 2759.8 ± 1278.7 N (Figure 2.10). This difference was not found to be statistically significant (p=0.73). The displacement to failure for the medial group was 11.3 ± 2.6 mm while the anterolateral group was 10.6 ± 2.2 mm. This difference was also not statistically significant (p=0.57). Audible cracking was heard prior to the load drop of 100N. At the end of the test, a visual inspection was conducted to confirm that permanent deformation of the fragments had occurred, where the fragments detached from the screws (Figure 2.11).

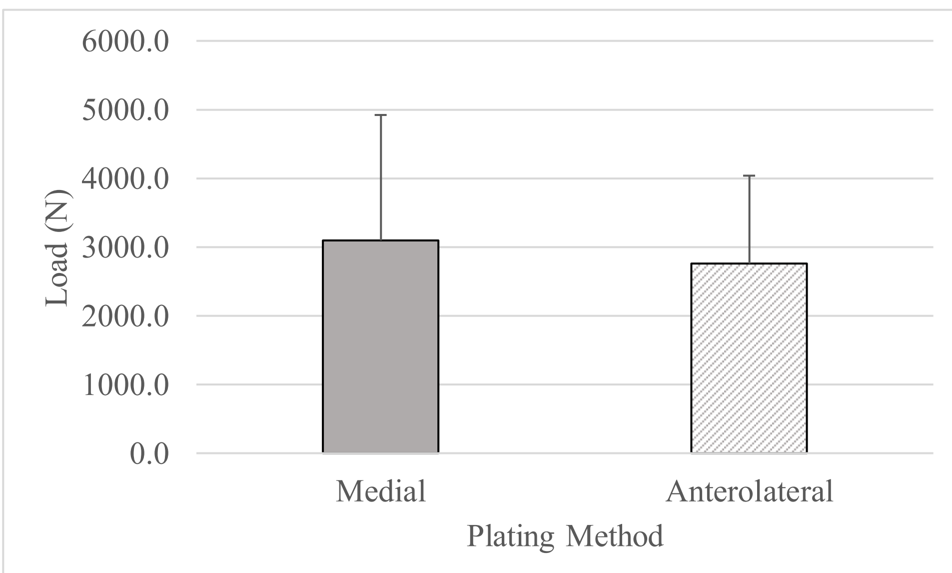

Figure 2.10: Load to Failure Results.
Comparison of the loads required to cause failure to the anterolateral and medial plated specimens (p = 0.98) (Specimen pairs 3-6 were used in this testing procedure, Table 2.1).

Figure 2.11: Permanent Deformation of Specimens.
Specimens were loaded to failure and permanent deformation was observed in each specimen.

2.4 Discussion

This is the first known study to measure the stiffness of the anterolateral and medial plating methods using a cadaveric model (with fibula) and a comminuted (pilon) fracture pattern. The use of cadaveric specimens in this study is a strength as it represents the variability seen in patients. To ensure evaluation of only the plating performance, a paired study was conducted, and the left and right specimens were shown to have had similar stiffnesses, thus allowing for a direct comparison of the anterolateral and medial plates. The main finding from this study was that the construct repaired with a medial plate tended to be 24% stiffer than the anterolateral plate; however, this difference was not found to be statistically significant.

To maintain consistency between specimens, plating was done prior to fracturing and a saw was used to create the fractures but, this is artificial and may not be representative of real-life fractures. A second synthetic talus was created due to the narrowing of the joint space after fracturing. Although the plating was completed prior to fracturing, the tightening of the screws caused small changes. In clinical practice, a surgeon may push the bone fragments more in real life or change their course of treatment based on soft tissue. However, these considerations were beyond the scope of this study.

The loads chosen for this study were based upon previous studies (Pirolo et al., 2015) and the estimated post-operative loading (Tschegg et al., 2008). Previous studies that modeled an extra-articular fracture loaded the specimens to 400 and 700 N (Pirolo et al., 2015; Yenna et al., 2011). For the intact specimens, 1400 N was selected at the maximum load level as it is the estimated magnitude of load a 95 kg patient may undergo during post-operative conditions (based upon 1.5 times bodyweight) (Tschegg et al., 2008). Comminution at the ankle joint causes instability, thus requiring a lower load. This was seen in the present study, as the same amount of deformation occurred at a load of 1400 N for the intact specimens as 400 N for the repaired specimens. The selected load levels of 400N may not be high enough to accurately represent what a patient experiences during post-operative loading. However, realistically, each fracture case is different and the loading each patient would experience may also be different depending on the healing rate, pain, and soft tissue considerations. Future studies investigating the stiffness of fracture fixations should also take the amount of deformation into consideration.

The medial plated specimens were found to be stiffer for five out of the six pairs; however, this difference was not found to be statistically significant ($p=0.28$). A power analysis (power =

0.80) showed that 19 specimens would be required in each group to reach statistical significance. This is an unreasonable number of specimens for this type of study due to cost and previous studies have used a sample size of three and four (Pirolo et al., 2015; Yenna et al., 2011). The specimens used in this study were from an older population and a pilon fracture is typically seen in younger patients. As this is a paired study, differences in age and sex is unlikely to affect the results. Statistical difference is different from clinical difference, and for some patients these results may still represent an improvement.

The trends observed herein agree with the suggestion that the plate be placed on the tension side of the fracture (medial for a varus fracture type fracture), which is based upon the orientation of the fracture in the coronal plane at the time of injury (Wei et al., 2014). Previous studies have also found the medial plate to be stiffer (Figure 2.12). Yenna et al. (2011) and Pirolo et al. (2015) both evaluated the stiffness of the anterolateral and medial plate using a synthetic tibia with an extra-articular fracture pattern. Yenna et al. (2011) concluded that the stiffness of the medial was greater than the anterolateral plate, based on axial loading to 400N (293.5 ± 38.9 N and 126.3 ± 46.6 N, respectively). The difference in stiffness values between Yenna et al. (2011) and the present study could be a result of a difference in fracture patterns. Pirolo et al. (2015) also used a different fracture pattern and loaded their specimens to 700N for three cycles (medial: 6211 ± 3147 N, anterolateral: 1290 ± 652 N). It is expected that an increase in load would result in a greater stiffness value, which may explain the differences when compared to the present study and the study conducted by Yenna et al. (2011).

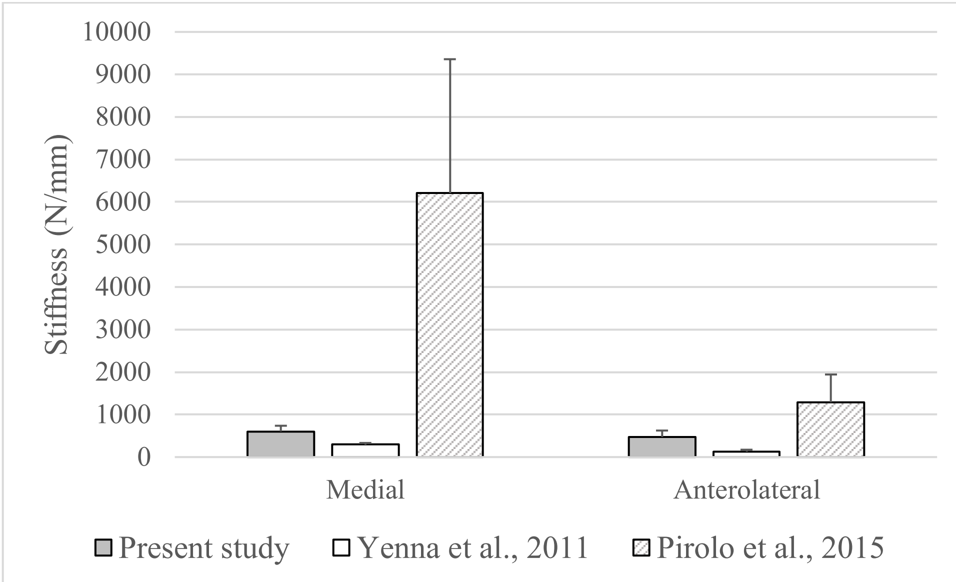

Figure 2.12: Comparison of Results to Previous Studies.
Comparison of stiffness values between the present study and the studies conducted by Yenna et al. (2011) and Pirolo et al. (2015).

The medial plated specimens were found to be stronger for four of the six pairs; however, this difference was not statistically significant. It may be that the medial plate showed greater strength due to the ability of the screws to secure the bone fragments. Upon visual inspection after the test, the medial plates tended to have a greater displacement of the anterolateral and posterolateral bone fragments, while the anterolateral plate tended to have a greater displacement of the medial fragment. Plate bending was observed in both the anterolateral and medial plated specimens. It is likely that the positioning of the screws contributed to the displacement of the bone fragments. The anterolateral plate had four screws on the anterior side of the bone, with the medial screw often barely securing the medial fragment. In contrast, the medial plate had four screws along the medial side of the tibia (two distal and two proximal) that were better able to capture all of the bone fragments. Pirolo et al. (2015) also did not find a significant difference between the plates when loaded to failure when comparing the displacement to failure or the ultimate load.

During the failure testing, the alignment method used could have affected how the articular surface was loaded potentially causing one of the bone fragments to be loaded more than another. However, at the beginning of each test, careful consideration was taken to ensure the actuator was distributed across the artificial talus.

2.5 Conclusion

This study demonstrated that the medial plate had a greater stiffness and strength when compared to the anterolateral plate, but neither of these were found to be statistically significant. However, this result does agree with previous findings and may reach significance with increased sample size. These results are only valid for the fracture pattern used in this study and may vary for a different fracture pattern. A surgeon should still consider the soft tissue and vascular injuries of the patient when selecting a plate.

This study helps to fill the gap of providing an assessment of these plates using cadaveric tibiofibular syndesmosis' and a pilon fracture pattern. This study solely assesses the biomechanical characteristics of the anterolateral and medial plates when used to treat pilon fractures. By understanding the biomechanical characteristics of these plates, it will help guide surgeons when treating pilon fractures as they may have more evidence for selecting which plate to provide a patient.

Chapter 3: The Use of an Optical Tracking System for Monitoring Interfragmentary Motion in Pilon Fractures

3.1 Introduction

Pilon fractures are caused by axial loads transmitted to the ankle through the foot and are characterized by comminution to the distal tibia. Currently, open reduction and internal fixation (ORIF) is used to treat pilon fractures, involving an operative procedure where a surgeon reduces the fracture and secures the fragments with either a medial or an anterolateral plate. The surgical plate bridges the fracture gap, providing stability to the fracture site, where the level of stability at the fracture site determines the type of bone healing. For secondary bone healing to occur, a strain of 2-10% has been recommended (Egol et al. 2004).

As stiffness has been the primary method of evaluating fracture stability post repair, a previous study compared assessments using stiffness to those of fracture gap motion, with a primary outcome of predicting callus formation (Elkins et al. 2016). Based on experimental and numerical testing, they concluded that 3D fracture motion is a better predictor and should be used to evaluate fracture fixation systems. This study focused on a comminuted supracondylar femoral fracture modeled on synthetic composite bones.

3D tracking systems have been previously configured to measure fracture gap motions (on the order of 0.06 mm to 0.3 mm, Muizelaar 2012); however, this study was only on a simple fracture using synthetic composite bones. Evaluating interfragmentary motion would complement stiffness testing typically conducted.

To date, there have been no known studies investigating the 3D motions of bone fragments for an intra-articular fracture using optical tracking technology. The purpose of this study was to configure an optical tracking system to quantify interfragmentary motion for the purposes of assessing the stability of varus type intra-articular pilon fractures treated with anterolateral and medial plates.

3.2 Methods

3.2.1 Specimen Preparation

Four pairs of lower leg cadaveric specimens (Specimen pairs 3-6 from Table 2.1) were used in this section of the project (mean age 77.5 ± 11.6 years, one male and three female). The method for preparation is described in (Section 2.2.1).

3.2.2 Camera Frame Design[4]

A frame was needed to support the cameras, at the appropriate distance and position, with minimal motion during testing, and to fit around the structure of the materials testing machine. Four cameras (Flex 13, OptiTrack, Natural Point Inc., Corvallis, OR) were used in this study and at least two cameras had to see each marker at all times. Therefore, cameras had to be placed around the entire machine. A smaller capture volume helps to increase the accuracy of precision tracking and was created by placing the cameras around the materials testing machine, as close to the specimen as possible, without obstructing the materials testing machine.

---

[4] Camera frame dimensions are in APPENDIX D: Camera Frame Drawings

The cameras were mounted on a preliminary camera frame and a static and dynamic test were performed to measure the vibrations from the materials testing machine. For the static test (machine not moving), a potted wood sample was placed in the materials testing machine with a marker placed on a 3D printed object nearby and the cameras collected data for 5 seconds. For the dynamic test, the wood sample was loaded using the protocol from Section 2.2.4. The change in position of the marker was measured and the marker was noted to recorded motion (even though stationary), indicating that there was camera frame motion from vibration, and, as a result, a new frame was needed.

The new camera frame was designed to provide rigid fixation for mounting the cameras (Figure 3.1). The camera frame consisted of 1" steel tube, welded together and painted black, that bolted to the materials testing machine. To test the new frame, the same test for the original frame was performed and the change in the position of the marker was re-measured.

3.2.3 Camera Setup

Four optical tracking cameras were fixed onto the camera frame around the materials testing machine. Black paint and fabric were used to cover any reflective surfaces within the capture volume, as this can disrupt the ability of the cameras to detect the reflective markers (diameter = 3 mm). The field of view of the cameras focused on the distal end of the specimen.

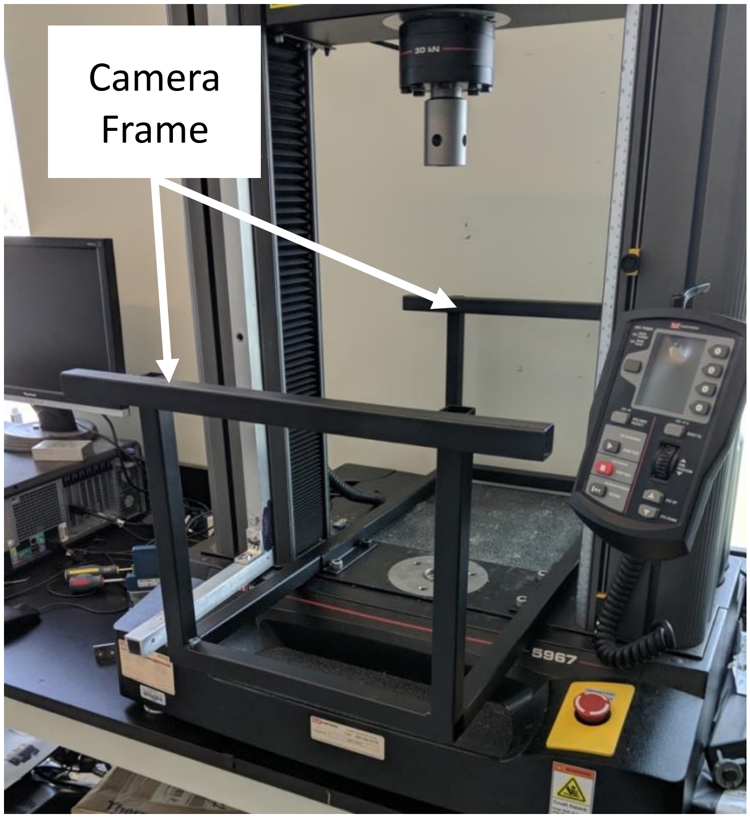

Figure 3.1: Frame for the Optical Tracking Cameras.
A camera frame was built to provide a rigid fixation for the cameras to minimize the vibrations experienced by the cameras.

A calibration wand (Figure 3.2(A)) (CWM-125 Calibration Wand, OptiTrack, Natural Point Inc, Corvallis, OR) was used to register the cameras relative to each other by moving the wand within the calibration volume. The software (Motive, Optitrack, Natural Point Inc., Corvallis, OR) calculated the relative positions of the cameras and reported the total estimated amount of error for the system. Next, the calibration square (Figure 3.2(B)) (CS-200 Calibration Square, OptiTrack, Natural Point Inc, Corvallis, OR) was used to set the origin for the global coordinate system. For every calibration, it was placed along the edge of the Instron, with the end touching the camera frame to set the origin for the global coordinate system (Figure 3.3).

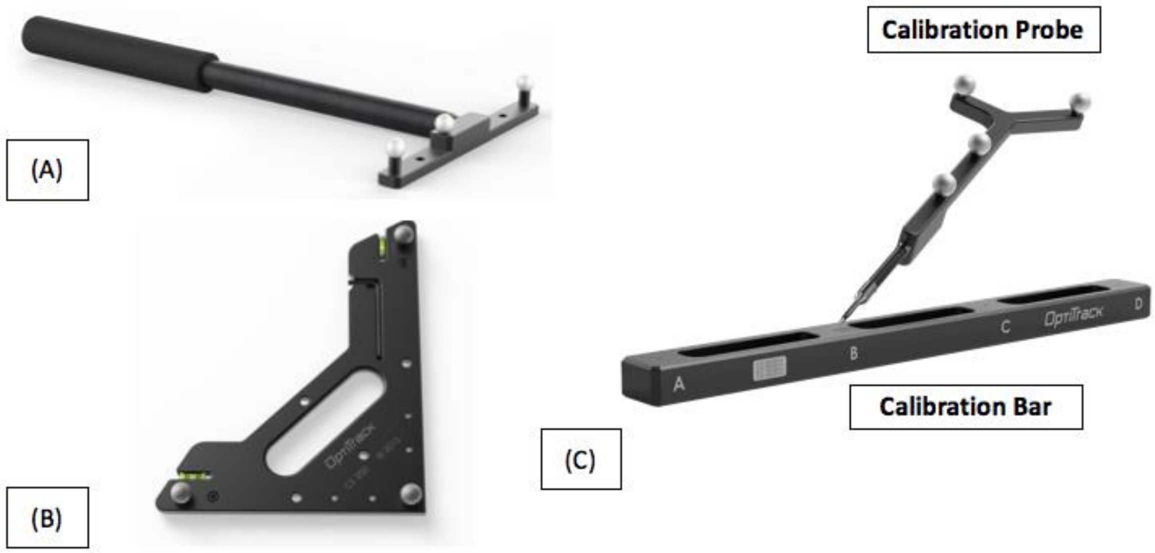

Figure 3.2: Calibration Tools for the OptiTrack Motion Tracking System.
(A) The calibration wand was used to register the cameras relative to each other around the capture volume. (B) The calibration square was used to establish a global coordinate system for the cameras. (C) The calibration probe and bar were used to create virtual point on the specimen. (https://optitrack.com/products/tools/).

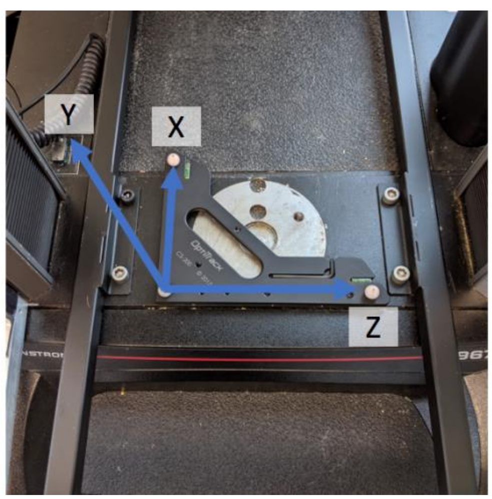

Figure 3.3: Position of the Calibration Square.
The calibration square defined the position of the global coordinate system. The position of the calibration square was placed along the edge of the Instron and in line with the camera frame for every calibration.

A digitizing probe (Figure 3.2(C)) (MSP0001 Digitizing probe, OptiTrack, Natural Point Inc., Corvallis, OR) was used in this study to identify virtual points on the specimen. Virtual points are locations identified during the calibration process, which can be used to calculate positions of these points throughout the trial without placing markers on them, based upon rigid body motion of the object. Calibration of the probe was completed by maintaining the position of the probe within a predetermined hole on the calibration bar (CB-300 Calibration Bar, OptiTrack, Natural Point Inc., Corvallis, OR) and then rotating it in a circular motion. This process allowed the software to precisely compute the tip location with reference to the markers on the probe. Calibration took place before testing each specimen and the estimated amount of error of the tip location was reported by the system.

3.2.4 Testing Set-up

Six unique marker clusters were created by joining cotter pins and using hot glue to secure the cotter pins and the markers onto the cluster (Figure 3.4). A minimum of three non-collinear markers was needed to establish a segment fixed coordinate system. After pilot testing with three, a fourth marker was added to each cluster to create redundancy if marker dropping occurred.

A drill (diameter = 1/16”) was used to create a hole in each of the five bone fragments: anterolateral, medial, posterolateral, distal fibula and proximal fibula. The marker clusters were placed in these holes and then secured with hot glue and painted black to minimize reflections. The specimen was loaded into the materials testing machine (Figure 3.5). Next, ten virtual points were identified on the specimen using the calibrated digitizing probe. The virtual points were picked to define the distal and proximal points along three fracture lines: anterior, posterior, and fibula (Figure 3.6).

The specimens were loaded according to the protocol described in Section 2.2.4 including loading to failure at a rate of 0.1 mm/s. Failure was defined as a load drop of 100 N or visible hardware failure. The optical tracking system collected samples at a rate of 120 FPS and the initial and final position of the marker clusters were used to find the overall motions.

Figure 3.4: Marker Clusters Used for Tracking Motion of the Fragments.
Marker clusters were created by intertwining cotter pins with each other and then securing them in place with hot glue and attaching the markers at the ends.

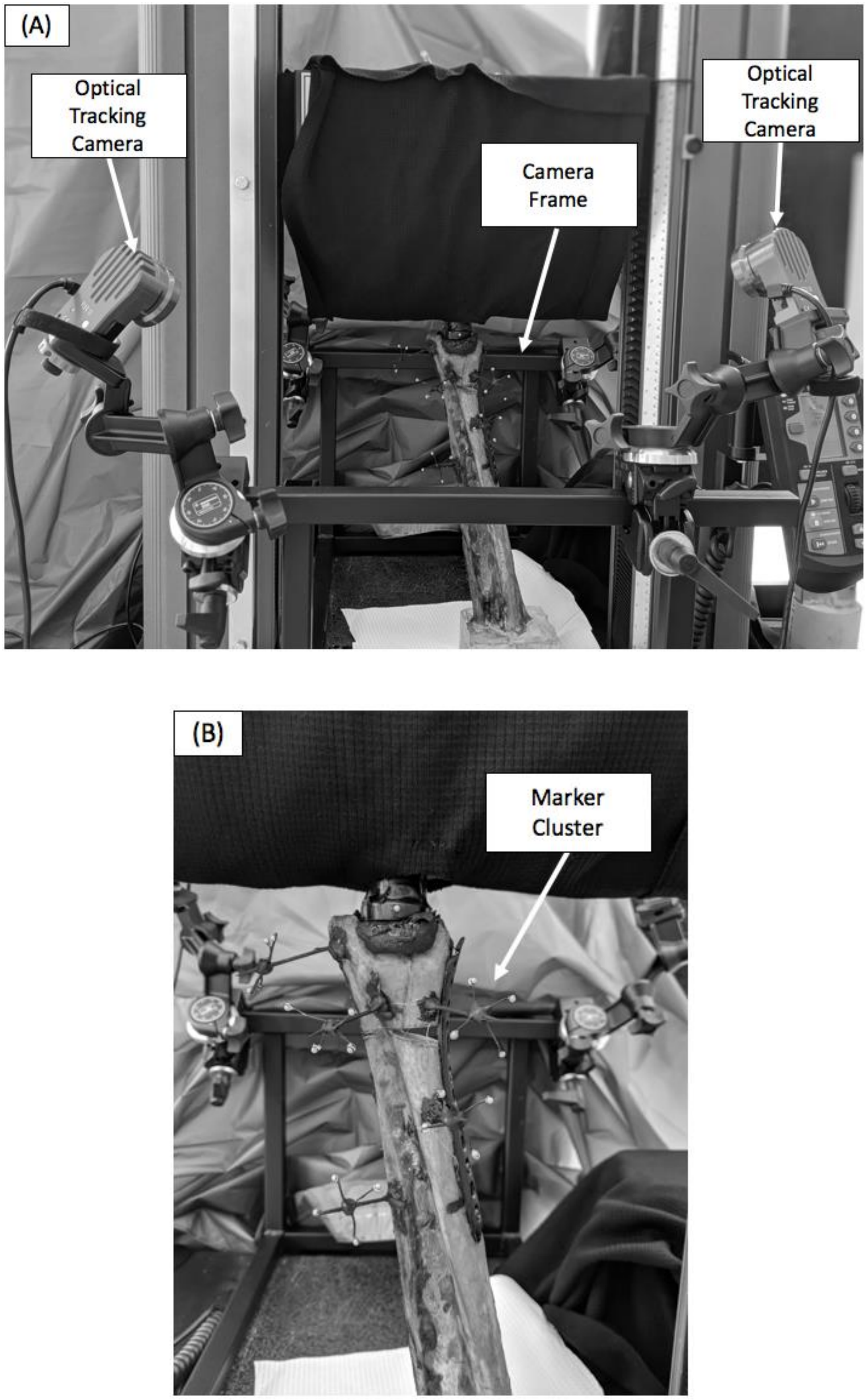

Figure 3.5: Optical Tracking Testing Set-up.
(A) Optical tracking cameras were mounted to the camera frame around the materials testing machine. (B) Specimen within the capture volume of the system with final placement of the marker clusters.

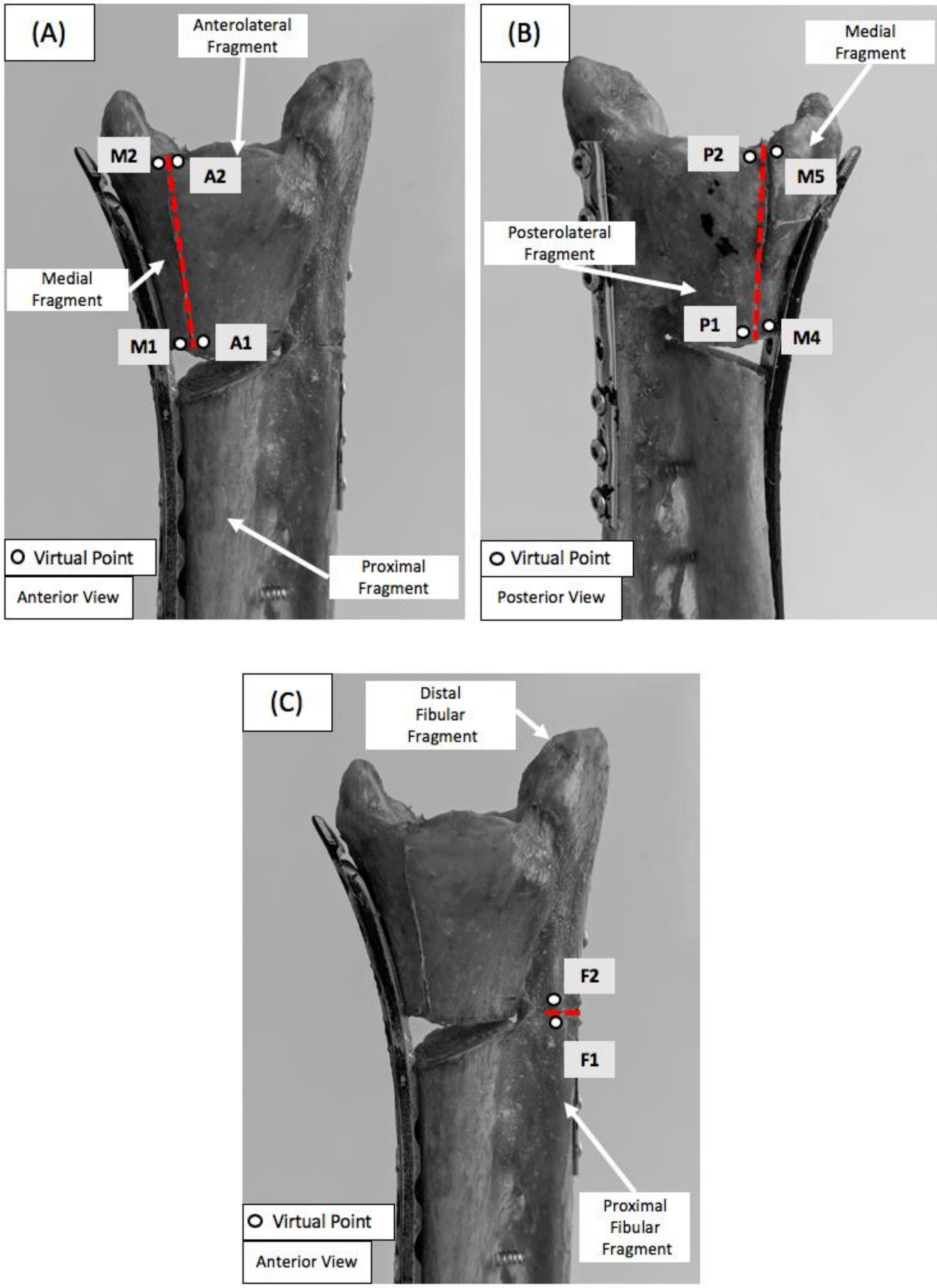

Figure 3.6: Virtual Points Collected During Calibration.
Virtual points were collected during the calibration trial for: (A) anterior fracture gap (B) posterior fracture gap and (C) fibula fracture gap.

3.3 Data Processing[5]

MATLAB (MATLAB_R2018b, MathWorks, Natick, MA) code was developed to calculate the overall motion at the ten virtual points (Figure 3.6). Three markers on each cluster were used to define the local coordinate system X', Y', Z' (Figure 3.7). At the first frame of data, a local coordinate system was created by finding the vector between P2 and P1 that defined the X' axis. A second vector was created between P3 and P1 that defined as the temporary Y' axis. The cross product of X' and temp Y' defined the Z' axis and the real Y' axis was found by taking the cross product of X' and Z' resulting in an orthonormal system of vectors. The projections were divided by their unit lengths to create the rotational matrix, R_1. Using this, each virtual point, A, was converted from the global coordinate system, X, Y, Z, to its respective fragment local coordinate system, X', Y', Z', ($\overrightarrow{P'}$) by subtracting $\vec{P}$ from the origin ($\vec{O}$) of the local coordinate system (marker 1) and multiplying it by R_1. This defined $\vec{P}$' for the first frame of data (Figure 3.8).

A new rotational matrix, R_n, was found for the last frame of data (end of test) using the same method as previously described, and the inverse, R_n', was found to transform the virtual point back into the global coordinate system. R_n' was multiplied by the sum of $\vec{P}$' and $\vec{O}$, converting the virtual point back into the global coordinate system. The magnitude ($\sqrt{X^2 + Y^2 + Z^2}$) between the original position of the virtual point and the translated point was calculated, representing the 3D motion of that point over the load to failure cycle, and captured both translational and rotational motions. A paired t-test ($\alpha = 0.05$) was used to compare each point on the medial plated specimens

[5] The code used for data processing is in APPENDIX E: MATLAB Code

to the same point on the anterolateral plated specimens when N = 4. Due to revision in the protocol and marker dropping, this could not be done on all points.

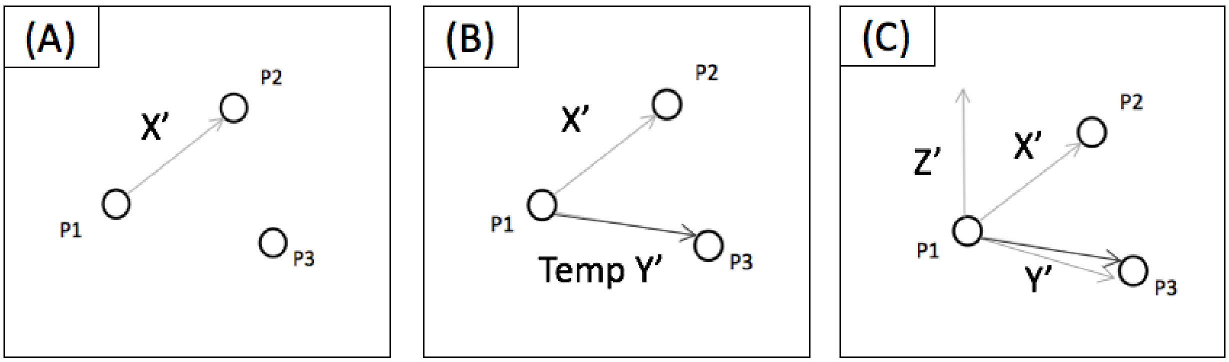

Figure 3.7: Defining the Local Coordinate System.
(A) The local coordinate system X’, Y’, Z’ was created by finding $\overrightarrow{\boldsymbol{P_{2\to1}}}$ to define the X’ axis. (B) The temporary Y’ axis was described as $\overrightarrow{\boldsymbol{P_{3\to1}}}$. (C) To define Z’, the cross product of $\overrightarrow{\boldsymbol{P_{2\to1}}}$ and $\overrightarrow{\boldsymbol{P_{3\to1}}}$ were found and the cross product of X’ and Z’ was found to define the true Y’ axis.

3.4 Results[6]

The net motion for the marker was decreased with the new frame design (Table 3.1). The mean error for the total system was 0.026 ± 0.005 mm and the mean error for location of the probe tip was 0.166 ± 0.024 mm.

[6] All images of specimen failure are shown in APPENDIX F: Specimen Failure Images

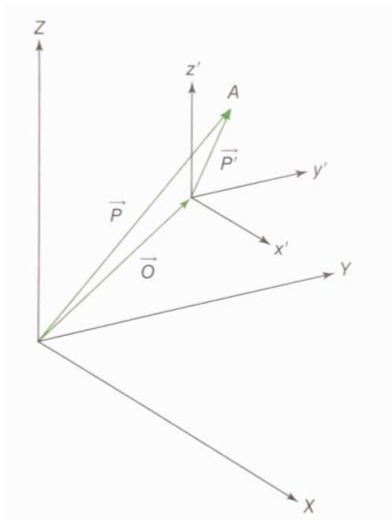

Figure 3.8: Converting Virtual Point A from the Global Coordinate System X, Y, Z, to the Local Coordinate System X', Y', Z'.
Virtual point A was converted to the local coordinate system X', Y', Z', by finding the rotational matrix describing the local coordinate system and multiplying it by $\overrightarrow{P} - \overrightarrow{O}$. To find the translated virtual point in the global coordinate system, the transformation matrix at the frame of failure was found. The inverse of the new R matrix was found and multiplied by $\overrightarrow{P'} + \overrightarrow{O}$ (Robertson, Caldwell, Hamill, Kamen, & Whittlesey, 2013).

Table 3.1: Net Results for the Vibrational Testing.
A marker was tracked while the materials testing machine was run, to quantify any errors induced through vibrations for the old and new frame design.

	Original	**New Frame**
Static Test (mm)	0.036	0.010
Dynamic Test (mm)	0.068	0.034

On the first pair tested not all points were digitized, and some had marker obstruction, therefore the number of samples used to calculate each points motion are indicated following the results in bracket. For the anterior fracture gap, the overall motions at the points A1, A2, M1, and M2 on the medial plated specimens were 10.6 ± 2.1 mm (N = 6), 10.8 ± 3.3 mm (N = 6), 12.9 ± 4.7 mm (N = 6), 11.2 ± 5.1 mm (N = 6), respectively (Figure 3.9). The overall motions for the anterolateral plated specimens at the points A1, A2, M1, and M2 were 14.5 ± 4.8 mm (N = 6), 12.1 ± 6.7 mm (N = 6), 28.8 ± 18.6 mm (N = 4), 18.5 ± 7.4 mm (N = 4), respectively (Figure 3.9). The movement at point A1 on the medial and anterolateral plated specimens (N = 6 per group) was found to be statistically different ($p = 0.03$). The movement at point A2 on the medial and anterolateral plated specimens (N = 6 per group) was not statistically different ($p = 0.65$). The movement at point M1 and M2 on the medial and anterolateral plated specimens (N = 4 per group) were not found to be statistically significant ($p = 0.30$ and $p = 0.41$, respectively).

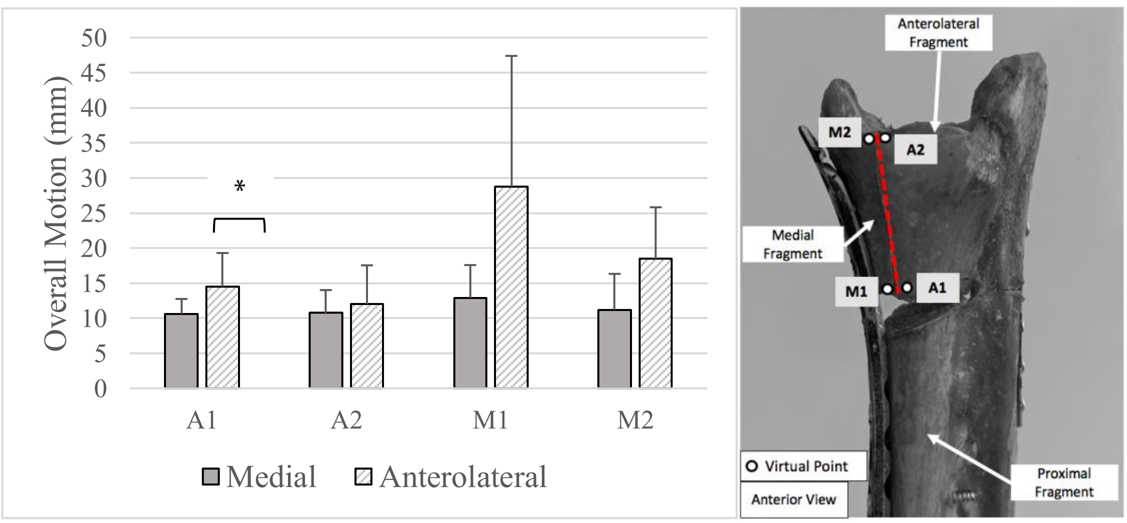

Figure 3.9: Overall Motion for the Anterior Fracture Gap.
Comparison of overall motion at the points along the anterior fracture gap, A1, A2, M1 and M2 for the anterolateral and medial plated specimens, where * indicated statistical significance ($p<0.05$).

For the posterior fracture gap, the overall motions at the points P1, P2, M4, and M5 on the medial plated specimens were 8.4 ± 2.8 mm (N = 5), 11.3 ± 7.3 mm (N = 5), 10.7 ± 4.8 mm (N = 6), 8.5 ± 3.1 mm (N = 6), respectively (Figure 3.10). The overall motions at the points P1, P2, M4, and M5 on the anterolateral plated specimens were 18.4 ± 0.12 mm (N = 2), 13.5 (N = 1), 27.3

± 14.1 mm (N = 4), 17.1 ± 5.4 mm (N = 4), respectively (Figure 3.10). Given the low sample size, no statistical analysis was conducted on points P1 and P2. The movement at point M4 on the medial and anterolateral plated specimens (N = 4 per group) was not statistically different (p = 0.20). The movement at point M5 on the medial and anterolateral plated specimens (N = 4 per group) was found to be statistically significant (p = 0.01).

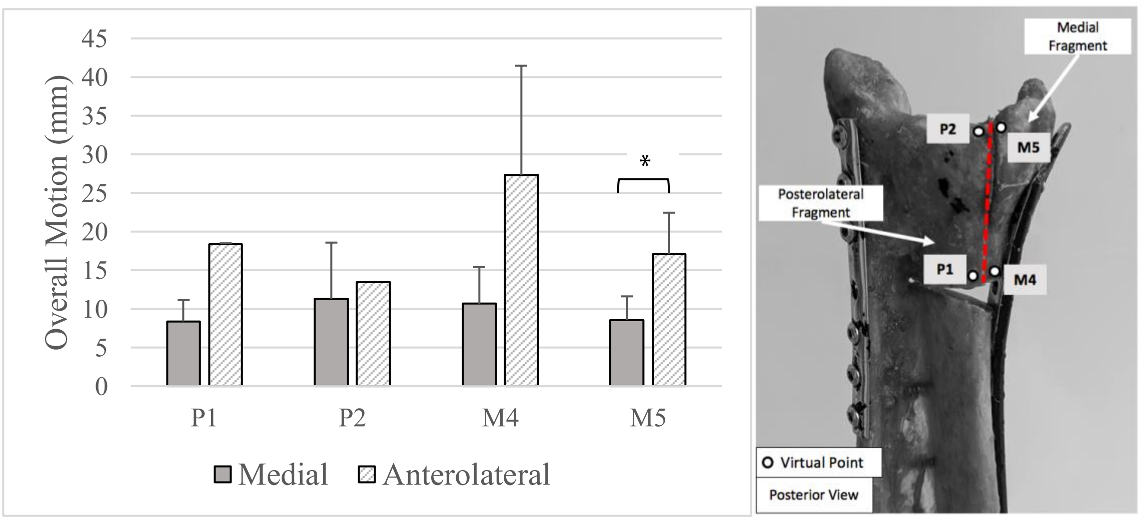

Figure 3.10: Overall Motion for the Posterior Fracture Gap.
Comparison of the overall motion at the points along the posterior fracture gap, P1, P2, M4 and M5 for the anterolateral and medial plated specimens, where * indicated statistical significance (p<0.05).

Two points, F1 and F2, were used to calculate the overall displacement of the fibula fracture gap. The overall motions at the points F1 and F2 on the medial plated specimens were 17.1 ± 20.85 mm (N = 5) and 7.9 ± 2.3 mm (N = 6), respectively (Figure 3.11). The overall motions at points F1 and F2 on the anterolateral plated specimens were 20.6 ± 15.0 mm (N = 6) and 12.7 ± 4.3 mm (N = 5), respectively (Figure 3.11). The movement at point F1 and F2 for the anterolateral and medial plated specimens (N = 5 per group) were not statistically different ($p = 0.98$ and $p = 0.24$, respectively).

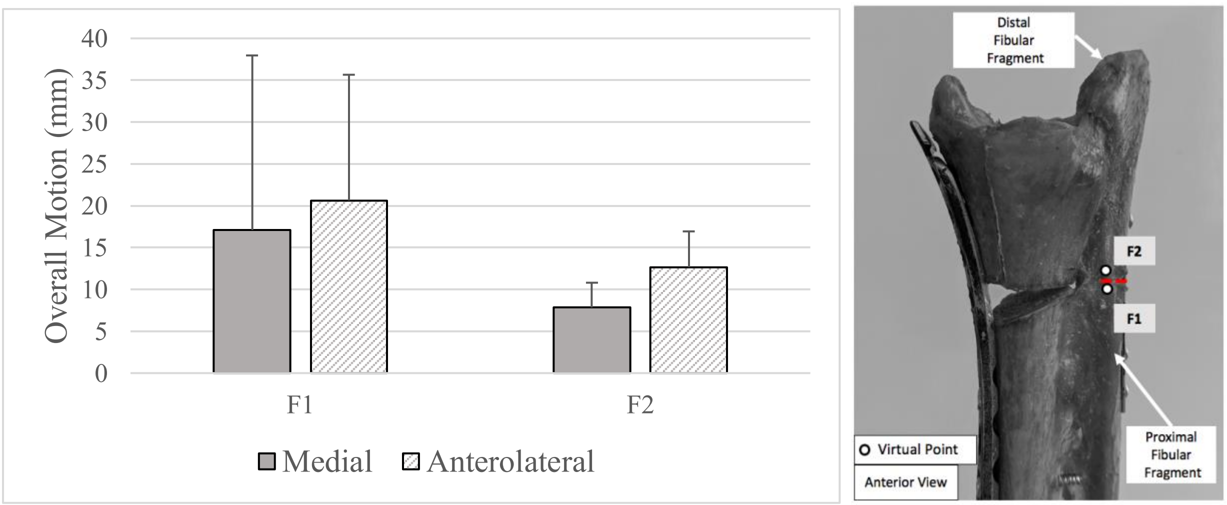

Figure 3.11: Overall Motion for the Fibula Fracture Gap.
Comparison of the overall motion at the points F1 (proximal) and F2 (distal), along the anterior side of the fibular fracture gap.

3.5 Discussion

Construct stiffness has historically been the primary mode of assessing fracture plates, but a recent study (Elkins et al., 2016) proposed that interfragmentary motion is more crucial for callus formation, and so the present study represents the first effort to look at the overall motion of the bone fragments for a comminuted distal tibia and fibula fracture using an optical tracking system.

As cameras were to be placed in close proximity to the moving materials testing machine, a test cycle was performed to determine the effects on the camera system. This study aimed to investigate the overall motions of the bone fragments, which were expected to be 5-10 mm and the error due to vibrations was less than 0.04 mm and therefore, could be considered negligible. The probe error was higher than expected; however, to improve this would require increasing the size of the calibration volume, which would increase the calibration error, so the capture volume was not changed.

At the anterior fracture gap, five of the six pairs had less motion at points A1 and A2 when treated with a medial plate and this difference was found to be statistically significant. Therefore, the medial plate provided greater stability to the anterior side of the anterolateral fracture fragment. Three out of the four pairs had less motion at points M1 and M2 when treated with medial plate. This is unsurprising, as the anterolateral plate only had one screw that caught the medial fragment, leaving it relatively unstable. Similarly, the overall motion for the medial plated specimens at point M4 was less than the anterolateral plated specimens for three of the four pairs. All four medial plated specimens had less motion when compared to anterolateral at point M5 and this difference was found to be significant. Therefore, it can be concluded that the medial plate reduced the amount of motion at point M5. The overall motion on the posterior side was expected to be greater for the anterolateral plated specimens as there was only one screw that held onto the bone fragment and often only partially grabbed the fragment. Surgeons should reconsider screw placement and orientation when patients are treated with an anterolateral plate to reduce the amount of displacement of the fragments. If too much displacement occurs, it could cause malunion or an increase in contact stress on the cartilage.

Several virtual points were unable to be tracked due to marker dropping, therefore limiting the sample size and the amount of statistical analysis that could be done herein. These issues were resolved on the latter pairs by adding a fourth marker to each cluster and further refined the painting and reflection management strategy. No clinical results may be extracted from these results yet, but additional testing is planned.

At the fibula fracture gap, four out of the five pairs showed less motion at points F1 and F2 when treated with a medial plate. A previous study investigated the motion of the distal tibiofibular syndesmosis using digital image correlation and found that tibiofibular syndesmosis was a slightly moveable joint as there was medial rotation of the fibula under axial loads (Hu et al. 2019). They recommended surgeons consider the biomechanical characteristics of syndesmotic joints. The motion of the fibula, in this present study, were expected to be the same in both groups given the same fibular fracture and plate were used, but this indicates the important interactions within the tibiofibular syndesmosis.

The use of motion tracking to evaluate interfragmentary motion has been limited. A previous study (Muizelaar, 2012) investigated the interfragmentary motion of periprosthetic fractures using a digital microscope (2D tracking) and compared it to a 3D motion tracking system. They found that the 2D method was more precise due to the lower standard deviations observed; however, the 3D motion tracking was able to provide more information about the motion of the fragments with less time for set-up. They recommended refining the system to improve the accuracy by optimizing the camera placement, the marker size and the number of cameras. These considerations were implemented in this present study. The cameras were repositioned for every specimen to ensure the cameras had complete visualization of the markers and was calibrated before every test.

Another study created a finite element model and performed a multivariate analysis to determine if the construct stiffness or 3D fracture gap motion was a better predictor of callus formation when locking plates are used to treat supracondylar femoral fractures (Elkins et al. 2016). Callus formation was found to be associated with constructs that favored longitudinal motion over transverse motion and that construct stiffness was not a suitable predictor of callus formation. This study suggested that fracture fixations should focus on 3D fracture-site motion as opposed to axial stiffness, highlighting the need for the present assessment. The results of the present study on interfragmentary motion, which support the use of a medial plate for varus fracture, do agree with the stiffness results from Chapter 2 but provide a more complete picture of the stability the fracture plates provide. However, the fracture line between the anterolateral and posterolateral bone fragments and the articular surface were unable to be evaluated due to obstruction. Based on the conclusions from previous work (Elkins et al. 2016), the 3D motion results from this present study should be taken into greater consideration. Therefore, further work is needed to explore the results of this study based on the motion in anatomical planes.

Two limitations arise from drilling holes in the bone to attach the marker clusters on the bone fragments. Firstly, by attaching the cluster to the bone, it is assuming that the bone fragment is a rigid body, meaning it is non-deformable. This is not true about bone; it is deformable and anisotropic. The virtual points likely had greater errors due to this rigid body assumption and potential small inconsistencies in where the points were digitized between specimens. However, the amount of deformation that the bone would undergo is minimal in comparison to the amount of displacement the fragments would experience. Furthermore, for the purpose of this study, attaching the clusters to the bone fragments allowed them to be secured in place at a distance from one other to reduce marker switching. Secondly, the process of drilling holes into the bone fragments could disrupt the integrity of the bone and could be a point of failure. However, due to the small diameter of the holes (1.5 mm), there were likely minimal effects on the mechanical integrity of the bone, and no visible fractures were noted surrounding the insertion point.

Finally, the overall motion of the bone fragments is dependent on where the load is applied. During normal gait, the load distribution and vector orientation is variable across the tibial plafond and will differ across patients. If the load were concentrated on one of the bone fragments, it would experience a greater amount of displacement in comparison to the other bone fragments. To reduce this error, when creating the bone cement mold of the articular surface, the actuator connector from the materials testing machine was placed on the mold prior to it solidifying. A bull's eye level was placed on top of the actuator to create a flat surface, allowing consistency being between the specimens. The results of the present could differ if the loading distribution were different (i.e. during ankle flexion and gait).

The optical tracking system was used to assess the initial and final positions of the points during failure testing. Most patients will never undergo conditions that cause failure; however, the motions that would induce secondary bone healing were unobservable by the optical tracking system. A strain of 2-10% has been found to induce secondary bone healing (Egol et al. 2004) however, this is dependent on the width of the fracture gap. A small fracture gap would have a higher amount of strain for less motion, while a larger fracture gap could withstand a greater amount of strain. The fracture gap in this study (0.58 mm), would need motion between 0.012 mm and 0.058 mm, which was unable to be detected by the optical tracking system. Therefore, the global movements found in this study cannot be correlated to the fracture strain. Furthermore, due to the comminuted fracture pattern, determining the strain at each fracture would be a substantial data analysis challenge. As there were multiple fractures that are not in line with the global coordinate system, an anatomical coordinate system would have to be created in order to break the strain into anatomical terms (e.g. shear and compression).

3.6 Conclusion

This difference in overall motion was found to be significant for two points and was not found to be statistically significant for the remaining points, likely due to the small sample size. Overall, there was a trend showing that the anterolateral plated specimens resulted in a greater amount of motion of the medial fragment when compared to the anterolateral plated specimens. This result was expected as the anterolateral plate does not capture the medial fragment as effectively as the medial plate, therefore providing less stability, which agrees with previous studies suggesting treating a varus fracture pattern with a medial plate. This study expands on previous studies investigating the effectiveness of the anterolateral and medial plates and is the first known study to investigate the 3D displacements of the bone fragments in an intra-articular fracture.

Chapter 4: General Discussion and Conclusions

4.1 Summary

Pilon fractures are a devasting injury that often disrupt the function of the ankle joint. The current treatment method for pilon fractures is open reduction and internal fixation, where a surgeon exposes the site of the fracture, reduces the fracture, and then treats it with either an anterolateral or medial plate. Typically, surgeons choose a plate based on the orientation of the fracture pattern in the coronal plane; hence medial for varus fracture pattern and anterolateral for a valgus fracture. Pilon fractures are often also associated with a fracture of the distal fibula. Frequently, patients who experience pilon fractures report poor outcomes, including pain and reduced function of the ankle. The purpose of this study was to evaluate the performance of the anterolateral and medial plates using a tibiofibular syndesmosis.

Six pairs of specimens (N=12) were divided into two groups, anterolateral plating, and medial plating. The left and right specimens were randomly placed into the two groups to compare the anterolateral and medial plates directly. The first objective of the thesis was to compare the construct stiffness and strength for anterolateral and medial plates when used to treat a varus fracture pattern. All specimens were potted and anatomical aligned, and a materials testing machine was used to apply five different loading sequences. The deformation and load at each maximum loading condition were outputted by the machine and used to calculate the stiffness. All specimens received a comminuted varus type pilon fracture as well as a fibula fracture. A medial or anterolateral plate was then used to treat the specimens. The same loading protocol for the intact specimens was used to test the stiffness for the repaired specimens, except testing was stopped at

400 N (similar amount of deformation observed in the intact specimens at 1400 N). The medial plate was found to have a higher stiffness than the anterolateral plate, but this difference was not found to be statistically significant. However, these results agree with previous literature (Pirolo et al., 2015). There was no statistical difference found between the strength of the medial and anterolateral plates; however, the medial plate was found to be stronger in five of the six specimens.

The second objective of this thesis was to use a motion tracking system to quantify the overall motion of the bone fragments during loading. The specimens were loaded to failure, defined as a load drop of 100N or hardware failure. Ten points on each specimen were analyzed and compared between the anterolateral and medial specimens. The results showed that the anterolateral plate had a higher level of overall motion of the medial bone fragment. This suggests that the medial plate would provide greater stability for the fragments when compared to the anterolateral plate. The overall motion of the bone fragments provided further insight into the stability that the plates provided. Three-dimensional fracture motion has been suggested to be a better predictor of callus formation, and therefore, should be considered when selecting plates to reduce the likelihood of malunion and non-union.

Overall, the results from the studies evaluating the construct stiffness and interfragmentary motion suggest that the medial plate tended to provide a greater level of stability when compared to the anterolateral plate when used to treat a varus type pilon fracture pattern.

4.2 Strengths and Limitations

The strengths and limitation of each individual study were detailed in their corresponding chapter. This section discusses the overall approach of the work as a whole.

Conducting a paired study using cadaveric specimens was a strength of this study. Previous studies have used synthetic tibias to assess the effectiveness of the anterolateral and medial plate. However, the use of a tibia and fibula syndesmosis allowed the assessment of the fibula, which is often fractured, and included the ligamentous structures between the tibia and the fibula. The cadavers were dissected to provide better control and visualization. It is possible that the surrounding soft tissue could have provided some more support, but this would likely have been equivalent to both plates.

Another strength of this study was assessing the plates using the current standard method (construct stiffness and strength) and a new technique (motion tracking). It was advantageous in this present work to assess the axial stiffness to observe differences in the previous studies conducted that used different fracture patterns and synthetic composite bones. Through the use of motion-tracking technology, the overall motion of the bone fragments was observed, which assessed the stability of the plates from a new perspective. Also, previous studies concluded that the 3D motion tracking was a more accurate predictor of callus formation than axial stiffness (Elkins et al., 2016). Therefore, the overall motion of the bone fragments should be the leading biomechanical factor when selecting a fracture fixation.

The clinical relevance of this project is also a strength of this study. Previous literature has used synthetic tibias to assess the effectiveness of the anterolateral and medial plate. Synthetic bones have the advantage of being less expensive and less variable than cadaveric specimens and pose no biohazardous risk. However, they lack the variability observed in the general population. By using cadaveric specimens, the ligamentous membranes connecting the tibia and the fibula added clinical relevance to the findings, in addition to, having an experienced orthopaedic surgeon complete the plating portion of this study.

The fracture pattern used in this study underrepresented the variability in fracture patterns observed in clinical practice. However, using a consistent fracture pattern and a paired study allowed a direct comparison of the plate stability and strength. Although not realistic, the fracture gap was controlled by creating the fractures with an oscillating saw and plating the specimens before the fracture to keep consistency.

The collaborating orthopedic surgeon chose a fracture pattern that most represented a pilon fracture in this study and, as such, should be representative of a large portion of these injuries. It is possible that, with a different fracture pattern, there may have been greater engagement in the medial fragment. The anterolateral would then be a more viable option, which may be what occurs in the portion of the population who are successfully treated. The findings in this study are only relevant to these plates, but likely transferable to other designs.

The sample size used for this study (N=12), was insufficient for achieving statistical significance. A power analysis (power = 0.80) showed that 19 specimens in each group would have been needed to reach statistical significance. This is an unrealistic number of specimens to use due to the associated costs of the specimens and hardware. However, the medial plates tended to be stiffer and provide a greater amount of stability when compared to the anterolateral plates, which is consistent with previous studies (Pirolo et al., 2015). These results may show some benefits to some patients.

Another strength of this study was evaluating the overall motion of comminuted fractures, at three fracture lines. This study developed a technique to detect motions relevant to immediate post-surgical loading. Due to obstruction, additional fracture lines were not evaluated. Although the techniques were successful for the three fracture lines, the process is quite labour intensive and highly sensitive to light and movement. The experimental set-up in this study minimized the errors, however, the resolution of the system limited the micromotion that could be detected. Therefore, the interfragmentary motion that would allow 2-10% strain was unable to be detected. Future studies should refine the camera and marker placements when working with an optical tracking system.

This study only assessed the stability and strength of the anterolateral and medial plates. However, in clinical practice, soft tissue considerations are an essential factor when treating pilon fractures. The results from this study aim to help guide surgeons when selecting a plate from a biomechanical perspective. However, the selected treatment method should consider the soft tissue.

4.3 Future Directions

Future work is needed to increase the sample size of this current study and then to repeat the study using a valgus fracture pattern. The same protocol would be used to assess the anterolateral and medial plates. This study provided benchtop recommendations that may inform clinical decisions for the selection of fracture fixations for treating pilon fractures with either an anterolateral or medial plate. The findings from this study could provide direction for a new design. The application of a motion capture system to fracture fixations could be applied to future work assessing the interfragmentary motion of various types of surgical fixations or other locations in the body.

4.4 Significance

This study assessed the biomechanical characteristics of the anterolateral and medial plate when used to treat varus type pilon fractures. The results of this study demonstrated that the medial plate tended to provide greater stability when compared to the anterolateral plate, from both a stiffness and a fragment motion perspective. This study provided further evidence to surgeons when treating pilon fractures, in hopes that the pain and function of the ankle joint post-surgery improve for the patients. Extra caution should be taken when using an anterolateral plate to ensure the medial fragment is secured, such that excessive motion of the fracture fragments does not occur. Furthermore, the motion capture techniques applied in this study have expanded the use of the technology to new areas and could be used to assess other types of fracture fixations.

References

Aneja, A., Luo, T. D., Liu, B., Domingo, M., Danelson, K., Halvorson, J. J., & Carroll, E. A. (2018). Anterolateral distal tibia locking plate osteosynthesis and their ability to capture OTAC3 pilon fragments. *Injury*, *49*, 409–413.

Barei, D. P., Nork, S. E., Bellabarba, C., & Sangeorzan, B. J. (2006). Is the absence of an ipsilateral fibular fracture predictive of increased radiographic tibial pilon fracture severity? *Journal of Orthopaedic Trauma*, *20*(1), 6–10.

Bear, J., Rollick, N., Helfet, D., & Bear, J. (2018). Evolution in Management of Tibial Pilon Fractures. *Current Reviews in Musculoskeletal Medicine*, *11*(4), 537–545.

Bonar, S. K., & Marsh, J. L. (1994). Tibial Plafond Fractures: Changing Pr inciples of Treatment. *Journal of the American Academy of Orthopaedic Surgeons*, *2*(6).

Casstevens, C., Le, T., Archdeacon, M. T., & Wyrick, J. D. (2012). Management of Extra-articular Fractures of the Distal Tibia: Intramedullary Nailing Versus Plate Fixation. *Journal of the American Academy of Orthopaedic Surgeons*, *20*(11), 675–683.

Cole, P. A., Mehrle, R. K., Bhandari, M., & Zlowodzki, M. (2013). The pilon map: Fracture lines and comminution zones in OTA/AO Type 43C3 pilon fractures. *J Orthop Trauma*, *27*(7), e152–e156.

Crist, B. D., Khazzam, M., Murtha, Y. M., & Rocca, G. J. Della. (2011). Pilon Fractures : Advances in Surgical Management. *Journal of the American Academ of Orthopaedic Surgeons*, *19*(10), 612–622.

Cushnaghan, J., & Dieppe, P. (1991). Study of 500 patients with limb joint osteoarthritis I. Analysis by age, sex, and distribution of symptomatic joint sites. *Annals of the Rheumatic Diseases*, *50*, 8–13.

Cutillas-Ybarra, M. B., Lizaur-Utrilla, A., & Lopez-Prats, F. A. (2015). Prognostic factors of health-related quality of life in patients after tibial plafond fracture. A pilot study. *Injury*, *46*(11), 2253–2257.

De-las-Heras-Romero, J., Lledo-Alvarez, A. M., Lizaur-Utrilla, A., & Lopez-Prats, F. A. (2017). Quality of life and prognostic factors after intra-articular tibial pilon fracture. *Injury*, *48*(6), 1258–1263.

Doblaré, M., García, J. M., & Gómez, M. J. (2004). Modelling bone tissue fracture and healing: A review. *Engineering Fracture Mechanics*, *71*(13–14), 1809–1840.

Egol, K. A., Kubiak, E. N., Fulkerson, E., Kummer, F. J., & Koval, K. J. (2004). Biomechanics of locked plates and screws. *Journal of Orthopaedic Trauma*, *18*(8), 488–493.

Elkins, J., Marsh, J. L., Lujan, T., Peindl, R., Kellam, J., Anderson, D. D., & Lack, W. (2016). Motion Predicts Clinical Callus Formation: Construct-Specific Finite Element Analysis of Supracondylar Femoral Fractures. *J Bone Joint Surg Am*, *98*(4), 276–284.

Garg, S., Khanna, V., Goyal, M. P., Joshi, N., Borade, A., & Ghuse, I. (2017). Comparative prospective study between medial and lateral distal tibial locking compression plates for distal third tibial fractures. *Chinese Journal of Traumatology - English Edition*, *20*(3), 151–154.

Grose, A., Gardner, M. J., Hettrich, C., Fishman, F., Lorich, D. G., Asprinio, D. E., & Helfet, D. L. (2007). Open reduction and internal fixation of tibial pilon fractures using a lateral approach. *Journal of Orthopaedic Trauma*, *21*(8), 530–537.

Hak, D. J., Toker, S., Yi, C., & Toreson, J. (2010). The Influence of Fracture Fixation Biomechanics on Fracture Healing. *Orthopedics*, *33*(10), 752–755.

Jacob, N., Amin, A., Giotakis, N., Narayan, B., Nayagam, S., & Trompeter, A. J. (2015). Management of high-energy tibial pilon fractures. *Strategies in Trauma and Limb Reconstruction*, *10*(3), 137–147.

Kojima, K. E., & Pires, R. E. S. (2017). Absolute and relative stabilities for fracture fixation: the concept revisited. *Injury*, *48*(6), S1.

Kuppa, S., Wang, J., Haffner, M., & Eppinger, R. (2008). Lower Extremity Injuriers and Associated Injury Criteria. *National Highway Traffic Safety Administration, USA*, *39*(5), 561–563.

Manninen, M. J., Lindahl, J., Kankare, J., & Hirvensalo, E. (2007). Lateral approach for fixation of the fractures of the distal tibia. Outcome of 20 patients: Technical note. *Archives of Orthopaedic and Trauma Surgery*, *127*(5), 349–353.

Marsell, R., & Einhorn, T. A. (2011). The Biology of Fracture Healing. *Injury*, *42*(6), 551–555.

Mauffrey, C., Vasario, G., Battiston, B., Lewis, C., Beazley, J., & Selgson, D. (2011). Tibial pilon fractures: A review of incidence, diagnosis, treatment, and complications. *Acta Orthopaedica Belgica*, *77*(4), 432–440. https://doi.org/10.1186/1471-2474-14-30

Muizelaar, A. (2012). Treatment of Periprosthetic Fractures of the Distal Femur Prototype Development for the Treatment of Periprosthetic Fractures of the Distal, 159.

Müller, M. E. (1987). Müller AO Classification of Fractures—Long Bones. *AO Foundation*, 1–7.

Norris, B. L., Lang, G., Russell, T. A. T., Rothberg, D. L., Ricci, W. M., & Borrelli, J. (2018). Absolute Versus Relative Fracture Fixation: Impact on Fracture Healing. *Journal of Orthopaedic Trauma*, *32*(3), S12–S16.

Pirolo, J. M., Behn, A. W., Abrams, G. D., & Bishop, J. A. (2015). Anterolateral Versus Medial Plating of Distal Extra-articular Tibia Fractures: A Biomechanical Model. *Orthopedics*, *38*(9), e760-5.

Robertson, G. E., Caldwell, G. E., Hamill, J., Kamen, G., & Whittlesey, S. (2013). *Research Methods in Biomechanics*.

Ruedi, T. P., Buckley, R. E., & Moran, C. G. (2007). *AO Principles of Fracture Managment*. *Thieme*.

Saltzman, C. L., Salamon, M. L., Blanchard, G. M., Huff, T., Hayes, A., Buckwalter, J. a, & Amendola, A. (2005). Epidemiology of ankle arthritis: report of a consecutive series of 639 patients from a tertiary orthopaedic center. *The Iowa Orthopaedic Journal*, *25*, 44–46.

Sfeir, C., Ho, L., Doll, B. A., Azari, K., & Hollinger, J. O. (2005). Fracture Repair. In *Bone Regeneration and Repair* (pp. 21–44).

Sitnik, A., Beletsky, A., & Schelkun, S. (2017). Intra-articular fractures of the distal tibia. *Acta Orthopaedica Scandinavica*, *2*, 352–361.

Teeny, S. M., & Wiss, D. A. (1993). Open Reduction and Internal Fixation of Tibial Plafond Fractures. *Clinical Orthopaedics and Related Research*, *NA;*(292), 108–117.

Tschegg, E. K., Herndler, S., Weninger, P., Jarnek, M., Stanzi-Tschegg, S., & Redl, H. (2008). Stiffness analysis of tibia-implant system under cyclic loading. *Materials Science & Engineering C-Biomimetic and Supramolecular Systems*, *28*(8), 1203–1208.

Vallier, H., Cureton, B., & Patterson, B. (2011). Randomized, prospective comparison of plate versus intramedullary nail fixation for distal tibia shaft fractures. *Journal of Orthopaedic Trauma*, *25*(12), 736–741.

Vallier, H., Le, T. T., & Bedi, A. (2008). Radiographic and clinical comparisons of distal tibia shaft fractures (4 to 11 cm proximal to the plafond): Plating versus intramedullary nailing. *Journal of Orthopaedic Trauma*, *22*(5), 307–311.

Viberg, B., Kleven, S., Hamborg-Petersen, E., & Skov, O. (2016). Complications and functional outcome after fixation of distal tibia fractures with locking plate - A multicentre study. *Injury*, *47*(7), 1514–1518.

Wei, S., Han, F., Lan, S., & Cai, X. (2014). Surgical treatment of pilon fracture based on ankle position at the time of injury/initial direction of fracture displacement: A prospective cohort study. *International Journal of Surgery*, *12*(5), 418–425.

White, R., & Camuso, M. (2012). Tibial Shaft Wedge Fractures.

Wolinsky, P., & Lee, M. (2008). The distal approach for anterolateral plate fixation of the tibia: an anatomic study. *Journal of Orthopaedic Trauma*, *22*(6), 404–407.

Yenna, Z. C., Bhadra, A. K., Ojike, N. I., ShahulHameed, A., Burden, R. L., Voor, M. J., & Roberts, C. S. (2011). Anterolateral and medial locking plate stiffness in distal tibial fracture model. *Foot & Ankle International / American Orthopaedic Foot and Ankle Society [and]*

Swiss Foot and Ankle Society, *32*(6), 630–637.

APPENDIX A: Glossary of Medical Terms from Merriam-Webster Dictionary[7]

Anisotropic: exhibiting properties with different values when measured in different directions: not isotropic

Anterior: situated near or toward the head or part most nearly corresponding to a head

Articular: of or relating to a joint

Callus: a mass of exudate and connective tissue that forms around a break in a bone and is converted into bone in healing

Cancellous: having a porous structure

Cartilage: a usually translucent somewhat elastic tissue that composes most of the skeleton of vertebrates embryos and except for a small number of structures (such as some joints, respiratory passages, and the external ear) is replaced by bone during ossification in the higher vertebrates

Comminution: to reduce to minute particles

Compact: having a dense structure or parts or units closely packed of joined

Coronal: of or relating to the frontal plane that passes through the long axis of the body

Diaphysis: the shaft of the long bone

Distal: situated away from the point of attachment or origin or a central point especially of the body

[7] * Definitions found from https://medical-dictionary.thefreedictionary.com

Dorsiflexion: flexion in a dorsal direction

Epiphysis: the usually rounded end of the shaft of a long bone that is composed mainly of cancellous bone covered by a thin layer of compact bone

*Extra-articular: situated or occurring outside of a joint

Frontal: parallel to the main axis of the body and at right angles to the sagittal plane

Hematoma: a mass of usually clotted blood that forms in a tissue, organ, or body space as a result of a broken blood vessel

*Intra-articular: within the cavity of a joint

Intramedullary: situated or occurring within a medulla

Lateral: of or relating to the side

Mal-union: incomplete or faulty union

Medial: extending toward the middle

Mesenchyme: loosely organized undifferentiated mostly mesodermal cells that give rise to such structures as connective tissues, blood, lymphatic, bone, and cartilage

Metaphysis: the transitional zone at which the diaphysis and the epiphysis of a bone come together

Non-union: failure of the fragments of a broken bone to knit together

Osteoarthritis: a common form of arthritis typically with onset during middle or old age that is characterized by progressively degenerative changes in the cartilage of one or more joints (as of the knees, hips, and hands) accompanied by thickening and overgrowth of adjacent bone and that is marked by symptomatically chiefly by stiffness, swelling, pain, deformation of joints, and loss of range of motion

Osteoblasts: a bone forming cell

Osteons: a Haversian canal with the concentrically arranged laminae of bone that surround it

Periosteum: the membrane of connective tissue that closely invests all bones except at the articular surface

*Pilon fracture: fracture of distal metaphysis of the tibia extending into the ankle joint

*Plafond: a ceiling, especially the ceiling of the ankle joint, that is, the articular surface of the distal end of the tibia.

Plantar-flexion: movement of the foot in which the toes flex downward toward the sole

Posterior: situated at or toward the hind part of the body

Proximal: situated next to or near the point of attachment or origin of a central point

Sagittal: of, relating to, situating in, or being the median plane of the body or any plane parallel to it

Strain: to cause a change of form or size in (a body) by application of external force)

Supracondylar: of, relating to, affecting, or being the part of a bone situated above a condyle

Syndesmosis: an articulation in which the contiguous surfaces of the bones are rough and are bound together by a ligament

Transverse: made at right angles to the long axis of the body

Valgus: of, relating to, or being a deformity in which anatomical part is turned outward away from the midline of the body to an abnormal degree

Varus: of, relating to, or being a deformity in which anatomical part is turned inward toward the midline of the body to an abnormal degree

APPENDIX B: Hardware Information

Table B.1: Specifications for the hardware used to plate one pair of specimens. (Left and right syndesmosis, two fibular plate and one anterolateral and medial plate). Label # corresponds to the labels in Figure B.1.

Label #	Quantity/ pair	Item Name
1	2	1/3 Tubular Plate (Fibula plate)
2	2	Cortical Screw ∅3.5 Length 16 mm
3	1	Cortical Screw ∅3.5 Length 18 mm
4	3	Cortical Screw ∅3.5 Length 14 mm
5	1	Locking Compression Plate Distal Tibia Plate (Anterolateral)
6	3	Locking Screw ∅3.5 Self-tap Length 36 mm
7	3	Locking Screw ∅3.5 Self-tap Length 38 mm
8	3	Locking Screw ∅3.5 Self-tap Length 40 mm
9	8	Cortical Screw ∅3.5 Length 30 mm
10	1	Locking Compression Plate Distal Tibia Plate (Medial)

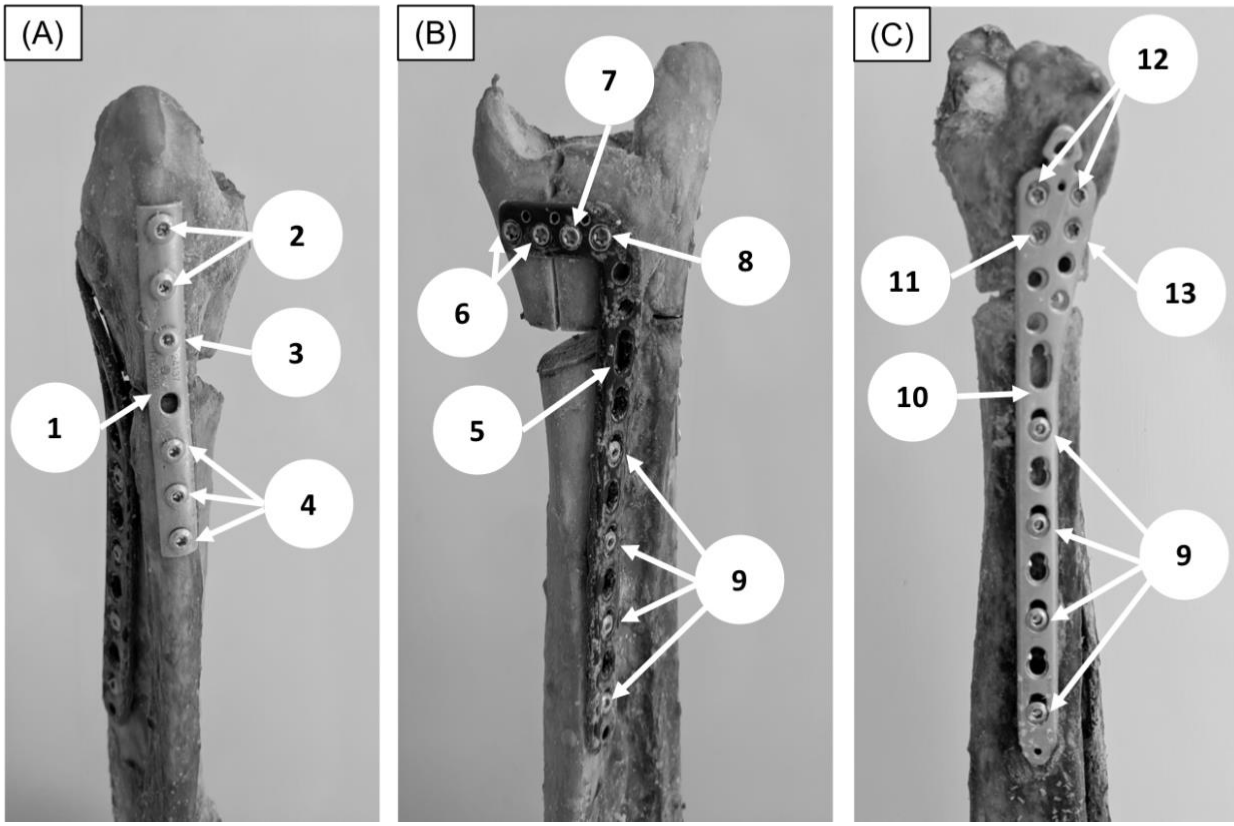

Figure B.1: Hardware Location on a Specimen.
Label # with description are listed in Table B.1.
(A) Fibula plated specimen and hardware (B) Anterolateral plated specimen and hardware
(C) Medial plated specimen and hardware.

APPENDIX C: Tabulated Data for Intact Specimen Testing

Table C.1: Average stiffness and deformation at the maximum loading sequences. The average stiffness value was calculated for all specimens at each loading sequence.

Max load level (N)	50	100	400	700	1000	1400
Average Stiffness (N/mm)	298.5	340.0	802.0	1102.5	1265.5	1433.2
Average Deformation (mm)	0.55	0.75	1.46	1.83	2.15	2.51

Table C.2: Intact stiffness (N/mm) values for the left and right specimen for each donor. Specimen pair 1-6 (Table 2.1) were used to find the intact stiffness for each specimen (MED = medial plate, ANT = anterolateral plate).

		1		2		3		4		5		6	
		L	R	L	R	MED	ANT	MED	ANT	MED	ANT	MED	ANT
Force (N)	50	287.7	245.4	194.9	194.9	310.7	438.6	399.4	308.6	331.2	305.7	281.3	290.5
	100	315.6	287.0	194.3	194.3	381.5	534.4	428.8	382.0	392.3	366.4	330.1	281.8
	400	678.1	745.8	733.6	733.6	915.6	1046.1	748.0	947.3	863.3	802.7	714.4	617.0
	700	884.8	834.3	1157.4	1157.4	1279.1	1331.0	1151.0	1297.1	1194.2	963.2	1034.9	941.8
	1000	1001.2	926.8	1355.1	1355.1	1397.1	1561.1	1275.9	1486.3	1402.0	1093.4	1235.0	1101.5
	1400	1119.7	1038.0	1490.7	1490.7	1617.3	1866.5	1304.6	1649.3	1638.4	1241.9	1428.8	1222.2

Table C.3: Repaired stiffness (N/mm) values for the left and right specimen. The left and right specimens were treated with either a medial or anterolateral plate, refer to Table 2.1 for designation (MED = medial plate, ANT = anterolateral plate).

		3		4		5		6		7		8	
		MED	ANT	MED	ANT	MED	ANT	MED	ANT	MED	ANT	MED	ANT
Force (N)	50	182.4	235.0	238.9	241.5	230.9	127.2	174.1	85.9	247.8	149.1	186.9	180.6
	100	219.7	295.4	294.3	274.6	246.7	136.4	179.1	82.5	305.8	178.9	210.0	210.0
	400	516.3	682.7	678.8	556.2	436.2	429.7	579.0	292.6	824.2	552.8	576.1	327.3

APPENDIX D: Camera Frame Drawings

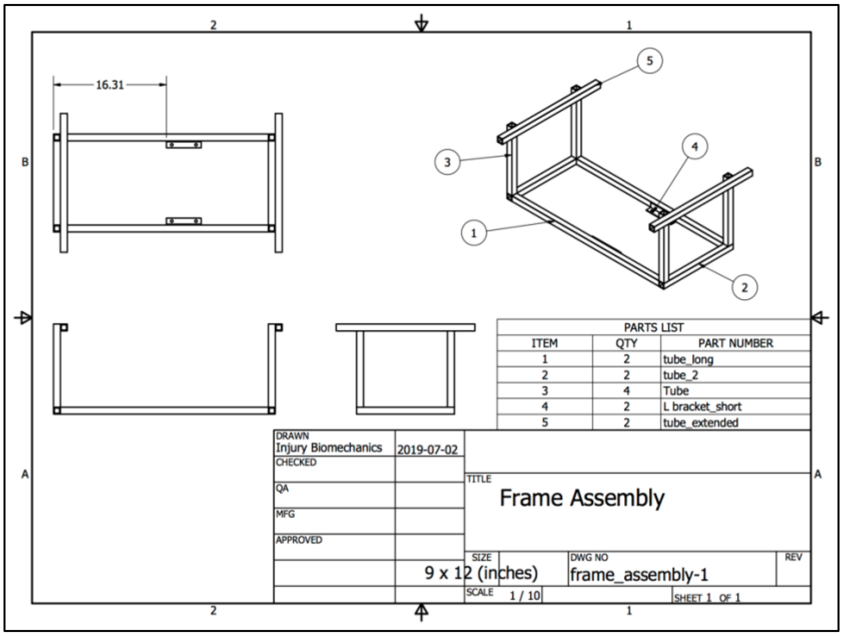

Figure D.1: Camera Frame Assembly Drawing.
Camera frame used for the motion capture cameras. All dimensions are in inches.

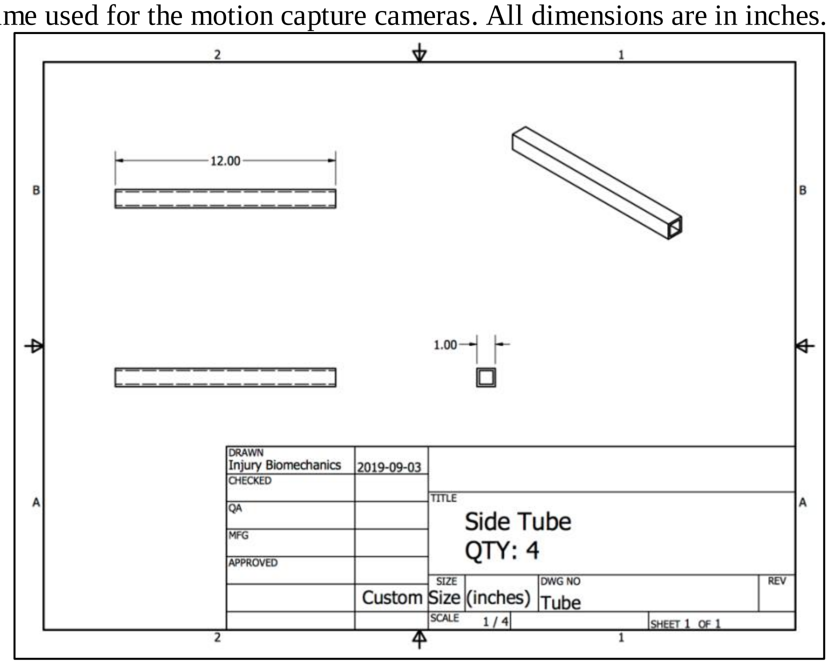

Figure D.2: Side Tube Drawing.
Part for the camera frame. All dimensions are in inches.

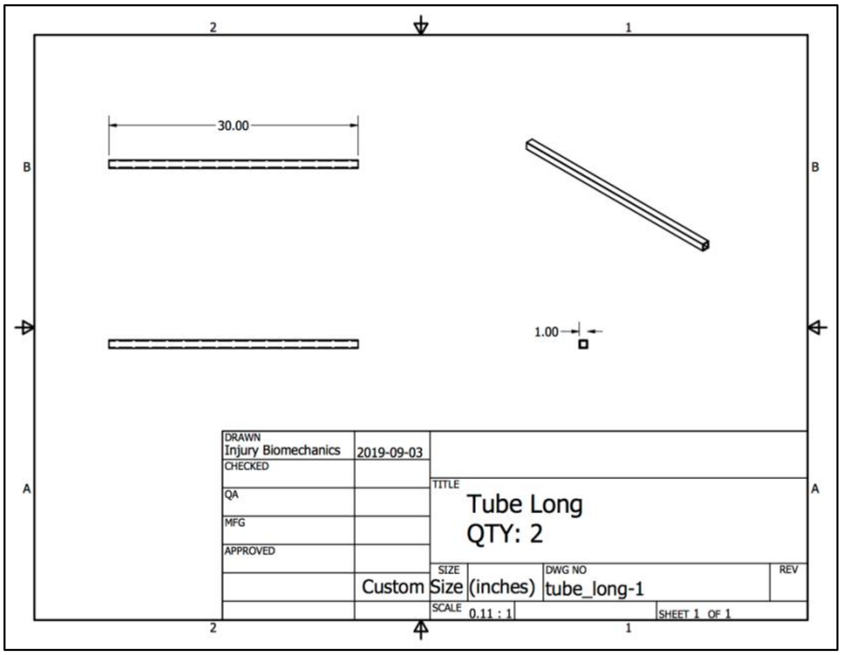

Figure D.3: Side Tube Drawing.
Part for the camera frame. All dimensions are in inches.

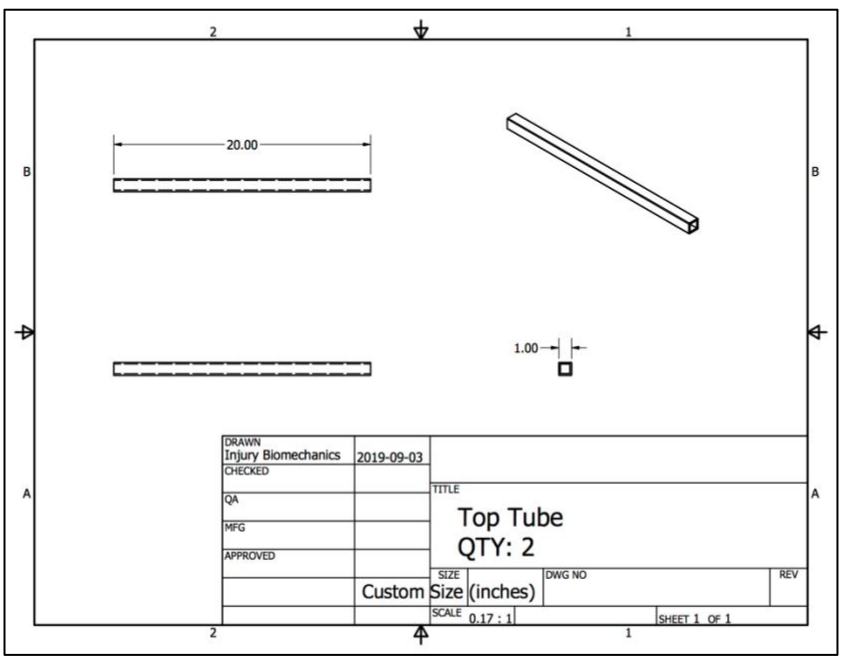

Figure D.4: Side Tube Drawing.
Part for the camera frame. All dimensions are in inches.

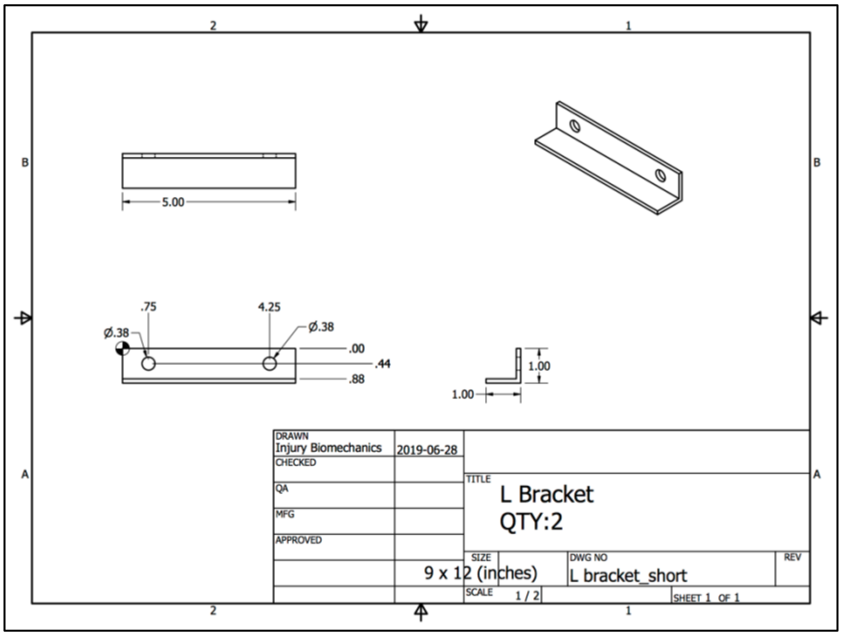

Figure D.5: Side Tube Drawing.
Part for the camera frame. All dimensions are in inches.

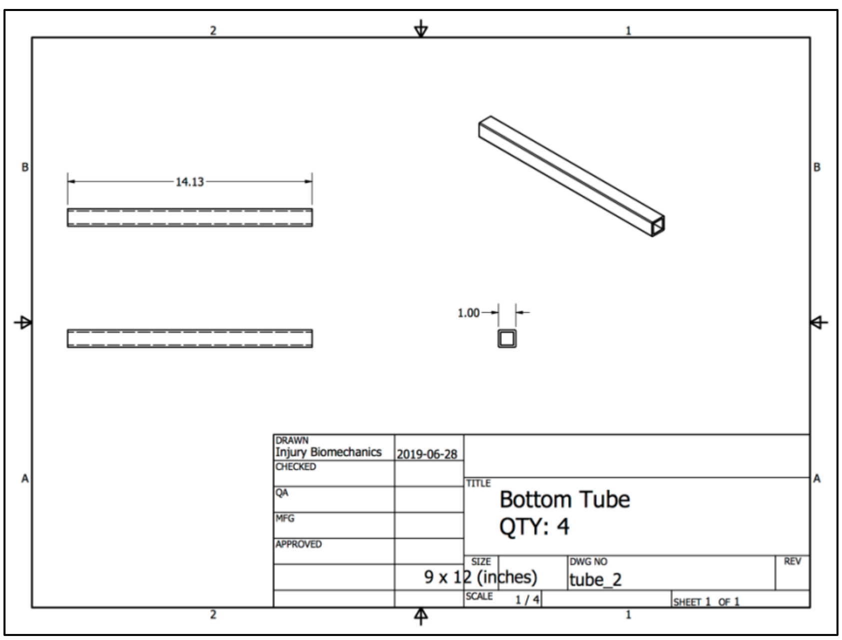

Figure D.6: Side Tube Drawing.
Part for the camera frame. All dimensions are in inches.

APPENDIX E: MATLAB Code

Main Code

```
%opts: takes the file and changes the setting for importing a csv file
opts = detectImportOptions('171545L_med_failure.csv'); % insert the file name
you want to work with
opts = setvartype(opts, 'double'); % changes text to cells
opts.DataLines = [8 inf]; %take the eighth row till the end
A = readtable('171545L_med_failure.csv',opts); %reading the table in
frame = table2array(A(1:41819,1)); %creating variable frame
time = table2array(A(1:41819,2));% creating variable time
T = table2array(A(1,:)); %creates an array with the first row of marker data
G = table2array(A(41819,:)); %creates an array for the last row of data
(motion stopped)

%%%%%%% Medial to VP 1
%Medial: creating an array for each marker, 3 columns correspond to
%the x,y, and z data
%Always need to use the variables marker_1, marker_2 and marker_3, make
%note of where marker dropping occured and marker_4 had to be used
marker_1 = T(:, 72:74); %cluster marker 4
marker_2 = T(:, 75:77);
marker_3 = T(:, 78:80);
virtual = T(:,84:86);  %virtual marker 1 for medial

%run the function unitvec55 to calculate the direct cosine matrix
[dcm] = unitvec55(marker_1,marker_2,marker_3);
B = marker_1'; %finding the transpose of marker 1
C = virtual'; %finding the transpose of virtual point
D = C-B; %fidning the difference between marker_1 and virtual
P_1 = dcm * D; %multiplying the difference by the dcm

%finding the unit vector for the last frame of data to find the
%displacement from initial to final
marker_1 = G(:, 72:74); %cluster marker 4
marker_2 = G(:, 75:77);
marker_3 = G(:, 78:80);

dcm = unitvec55(marker_1,marker_2,marker_3); %unit vector at the last frame
of data
Tmatrix_inv = dcm'; %inverse of the unit unit vector to translate the points
from local to global
P_result = Tmatrix_inv * P_1 + (marker_1(1,:)'); %putting the virtual point
back into global by adding P_1 and marker_1 (origin) and multiplying it by
the inverse matrix
P_result = P_result'; %finding the transpose of the virutal point

[V_mag] = MagVec55(P_result, virtual); %resultant magnitude for the original
place of the virutal marker to the translated point
M_med_prx = V_mag; %labelling the magnitude value
```

```
%This code is then repeated for the remaining nine points

%%%%%%%%%%%%%%%%%%%%%%%%%%%%%%%%%
%Medial to VP2
marker_1 = T(:, 72:74); %cluster marker 4
marker_2 = T(:, 75:77);
marker_3 = T(:, 78:80);
virtual = T(:,87:89);

[dcm] = unitvec55(marker_1,marker_2,marker_3);
B = marker_1';
C = virtual';
D = C-B;
P_1 = dcm * D;

marker_1 = G(:, 72:74); %cluster marker 4
marker_2 = G(:, 75:77);
marker_3 = G(:, 78:80);

dcm = unitvec55(marker_1,marker_2,marker_3);
Tmatrix_inv = dcm';
P_result = Tmatrix_inv * P_1 + (marker_1(1,:)');
P_result = P_result';

[V_mag] = MagVec55(P_result, virtual);
M_med_dis = V_mag;
%%%%%%%%%%%%%%%%%%%%%%%%%%%%%%%%%%%
%Medial to VP4
marker_1 = T(:, 72:74); %cluster marker 4
marker_2 = T(:, 75:77);
marker_3 = T(:, 78:80);
virtual = T(:,93:95);

[dcm] = unitvec55(marker_1,marker_2,marker_3);
B = marker_1';
C = virtual';
D = C-B;
P_1 = dcm * D;

marker_1 = G(:, 72:74); %cluster marker 4
marker_2 = G(:, 75:77);
marker_3 = G(:, 78:80);

dcm = unitvec55(marker_1,marker_2,marker_3);
Tmatrix_inv = dcm';
P_result = Tmatrix_inv * P_1 + (marker_1(1,:)');
P_result = P_result';

[V_mag, V_diff] = MagVec55(P_result, virtual);
M_med_prx_post = V_mag;
%%%%%%%%%%%%%%%%%%%%%%%%%%%%%%%%%%%
%Medial to VP 5
```

```
marker_1 = T(:, 72:74); %cluster marker 4
marker_2 = T(:, 75:77);
marker_3 = T(:, 78:80);
virtual = T(:, 96:98);

[dcm] = unitvec55(marker_1,marker_2,marker_3);
B = marker_1';
C = virtual';
D = C-B;
P_1 = dcm * D;

marker_1 = G(:, 72:74); %cluster marker 4
marker_2 = G(:, 75:77);
marker_3 = G(:, 78:80);

dcm = unitvec55(marker_1,marker_2,marker_3);
Tmatrix_inv = dcm';
P_result = Tmatrix_inv * P_1 + (marker_1(1,:)');
P_result = P_result';
A_med_prx = P_result - virtual;

[V_mag] = MagVec55(P_result, virtual);
M_med_dis_post = V_mag;
%%%%%%%%%%%%%%%%%%%%%%%%%%%%%%%%%%%%%%%%%%%%%
%Anterolateral to V1
marker_1 = T(:, 3:5);
marker_2 = T(:, 6:8);
marker_3 = T(:, 9:11);
virtual = T(:,15:17);

[dcm] = unitvec55(marker_1,marker_2,marker_3);
B = marker_1';
C = virtual';
D = C-B;
P_1 = dcm * D;

marker_1 = G(:, 3:5);
marker_2 = G(:, 6:8);
marker_3 = G(:, 9:11);

dcm = unitvec55(marker_1,marker_2,marker_3);
Tmatrix_inv = dcm';
P_result = Tmatrix_inv * P_1 + (marker_1(1,:)');
P_result = P_result';

[V_mag] = MagVec55(P_result, virtual);
M_ant_prx = V_mag;
%%%%%%%%%%%%%%%%%%%%%%%%%%%%%%%%%%%
%Anterolateral to V2
marker_1 = T(:, 3:5);
marker_2 = T(:, 6:8);
marker_3 = T(:, 9:11);
```

```
virtual = T(:,18:20);

[dcm] = unitvec55(marker_1,marker_2,marker_3);
B = marker_1';
C = virtual';
D = C-B;
P_1 = dcm * D;

marker_1 = G(:, 3:5);
marker_2 = G(:, 6:8);
marker_3 = G(:, 9:11);

dcm = unitvec55(marker_1,marker_2,marker_3);
Tmatrix_inv = dcm';
P_result = Tmatrix_inv * P_1 + (marker_1(1,:)');
P_result = P_result';

[V_mag] = MagVec55(P_result, virtual);
M_ant_dis = V_mag;
%%%%%%%%%%%%%%%%%%%%%%%%%%%%%%%%
% %Posterolateral to V1
marker_1 = T(:, 102:104);
marker_2 = T(:, 105:107);%using cluster 4
marker_3 = T(:, 109:111);
virtual = T(:,114:116);

[dcm] = unitvec55(marker_1,marker_2,marker_3);
B = marker_1';
C = virtual';
D = C-B;
P_1 = dcm * D;

marker_1 = G(:, 102:104);
marker_2 = G(:, 105:107);% cluster 4
marker_3 = G(:, 109:111);

dcm = unitvec55(marker_1,marker_2,marker_3);
Tmatrix_inv = dcm';
P_result = Tmatrix_inv * P_1 + (marker_1(1,:)');
P_result = P_result';

[V_mag] = MagVec55(P_result, virtual);
M_pos_1 = V_mag;
%%%%%%%%%%%%%%%%%%%%%%%%%%%%%%%%
%Posterolateral to V2
marker_1 = T(:, 102:104);
marker_2 = T(:, 105:107);%using cluster 4
marker_3 = T(:, 109:111);
virtual = T(:,117:119);

[dcm] = unitvec55(marker_1,marker_2,marker_3);
B = marker_1';
```

```
C = virtual';
D = C-B;
P_1 = dcm * D;

marker_1 = G(:, 102:104);
marker_2 = G(:, 105:107);%using cluster 4
marker_3 = G(:, 109:111);

dcm = unitvec55(marker_1,marker_2,marker_3);
Tmatrix_inv = dcm';
P_result = Tmatrix_inv * P_1 + (marker_1(1,:)');
P_result = P_result';

[V_mag] = MagVec55(P_result, virtual);
M_pos_2 = V_mag;

%%%%%%%%%%%%%%%%%%%%%%%%%%%
% Distal Fibula to V1
marker_1 = T(:, 27:29); %%cluster marker 4
marker_2 = T(:, 30:32);
marker_3 = T(:, 33:35);
virtual = T(:,39:41);

[dcm] = unitvec55(marker_1,marker_2,marker_3);
B = marker_1';
C = virtual';
D = C-B;
P_1 = dcm * D;

marker_1 = G(:, 27:29); %%cluster marker 4
marker_2 = G(:, 30:32);
marker_3 = G(:, 33:35);

dcm = unitvec55(marker_1,marker_2,marker_3);
Tmatrix_inv = dcm';
P_result = Tmatrix_inv * P_1 + (marker_1(1,:)');
P_result = P_result';

[V_mag] = MagVec55(P_result, virtual);
M_fib_dis = V_mag;
%%%%%%%%%%%%%%%%%%%%%%%%%%%%%%%%%%%%%%%%
% Proximal Fibula to V1
marker_1 = T(:, 48:50);
marker_2 = T(:, 51:53); %%cluster marker 4
marker_3 = T(:, 54:56);
virtual = T(:,60:62);

[dcm] = unitvec55(marker_1,marker_2,marker_3);
B = marker_1';
C = virtual';
D = C-B;
P_1 = dcm * D;
```

```
marker_1 = G(:, 48:50);
marker_2 = G(:, 51:53); %%cluster marker 4
marker_3 = G(:, 54:56);

dcm = unitvec55(marker_1,marker_2,marker_3);
Tmatrix_inv = dcm';
P_result = Tmatrix_inv * P_1 + (marker_1(1,:)');
P_result = P_result';

[V_mag] = MagVec55(P_result, virtual);
M_fib_prx = V_mag;
%%%%%%%%%%%%%%%%%%%%%%%%%%%%%%%%%%%%%%%%
% create a table with the results and saves in an excel file
M = table([M_ant_prx], [M_ant_dis], [M_fib_dis], [M_fib_prx],
[M_med_prx],[M_med_prx_post], [M_med_dis], [M_med_dis_post],[M_pos_1],
[M_pos_2],'VariableNames',{'M_ant_prx', 'M_ant_dis', 'M_fib_dis', 'Fib_prx',
'Med_prx', 'M_med_prx_post','Med_dis', 'M_med_dis_post', 'Post_1', 'Post_2'})
writetable(M, '171545L_M_output.csv','Delimiter', ',')
type 171545L_M_output.csv
```

Function: unitvec55

```
%FUNCTION: creates the unit vector for the every frame of data for the defined
markers and the outputs the transformation matrix
%INPUT: Marker 1, Marker 2, Marker 3
%OUTPUT: DCM (direct cosine matrix

function [dcm] = unitvec55(marker_1,marker_2,marker_3) %callout of function

%calculate the unit vector of vector_i_1_2
vec_i = (marker_2(1,:) - marker_1(1,:))/norm(marker_2(1,:) - marker_1(1,:));

%calculate the midpoint between vector 1 & 2
%OM_1_2 = marker_1(1,:) + ((0.5)*vec_i);

%finding the vector between the midpoint and marker 3
vec_jtemp =
(marker_3(1,:) - marker_1(1,:))/norm(marker_3(1,:) - marker_1(1,:));

%cross the first two vectors to find the third vector
vec_k = cross(vec_i, vec_jtemp)/norm(cross(vec_i, vec_jtemp));
vec_j = cross(vec_k, vec_i)/norm(cross(vec_k, vec_i));

%check to see if the vectors are orthogonal by calculating the dot product
%(if it equals 0, than they are orthogonal)

ORG_ij = dot(vec_i, vec_j);
ORG_ij = round(ORG_ij,4); %rounding the product to 4 sigfigs
ORG_ik = dot(vec_i, vec_k);
ORG_ik = round(ORG_ik,4);
ORG_jk = dot(vec_k, vec_j);
ORG_jk = round(ORG_jk,4);
assert(ORG_ij ==0, 'Dot product is not zero') %checks that the dot product is
zero and the axis are orthogonal
assert(ORG_ik ==0, 'Dot product is not zero')
assert(ORG_jk ==0, 'Dot product is not zero')

%creating a matrix with the unit vectors (3X3 matrix)
dcm= [vec_i; vec_j; vec_k];
dcm;
end
```

Function: magvec55

```
%FUNCTION: Finds the magnitude fort the difference between the virtual point
and P_result
%%INPUT: two vectors and it will give the magnitude between them
%%OUTPUT: The magnitude of the vector between the two vectors
 function [V_mag] = MagVec(P_result, virtual);
   V_mag = sqrt(((P_result(1, 1) - virtual(1,1))^2)+((P_result(1,
2) - virtual(1,2))^2)+ ((P_result(1, 3) - virtual(1,3))^2));
```

```
   V_mag = V_mag*1000;
End
```

APPENDIX F: Specimen Failure Images

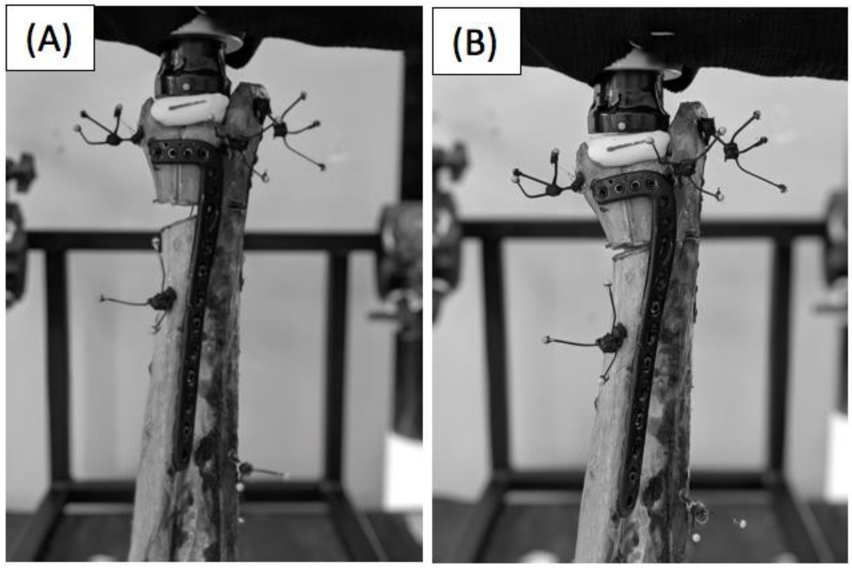

Figure F.1: Specimen 3 (Right) Failure Testing.
(A) Anterior view of initial position of the specimen (B) Anterior view of final position of the specimen.

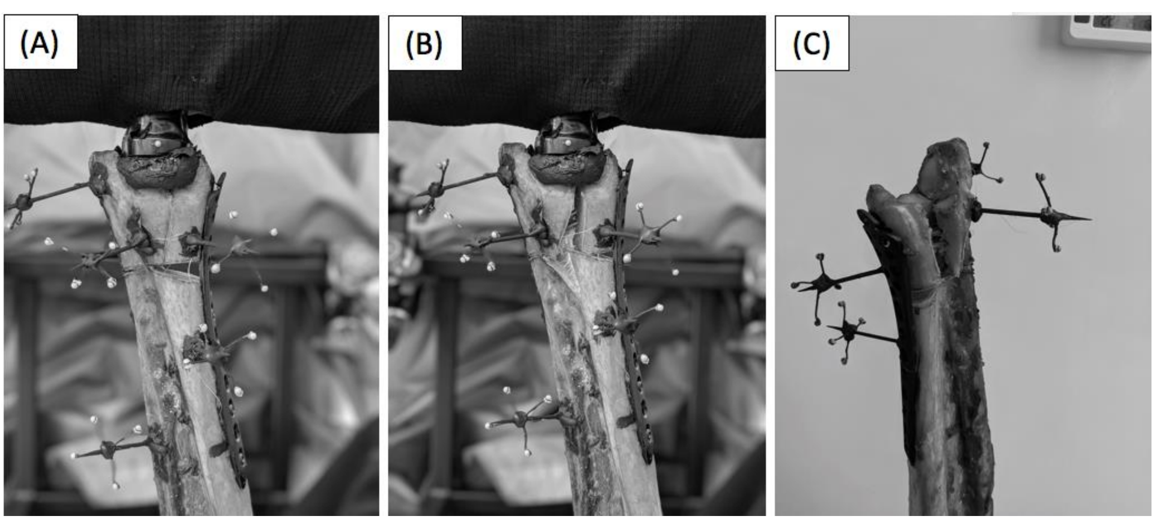

Figure F.2: Specimen 3 (Left) Failure Testing.
(A) Anterior view of initial position of the specimen (B) Anterior view of final position of the specimen (C) Posterior view of fragment failure.

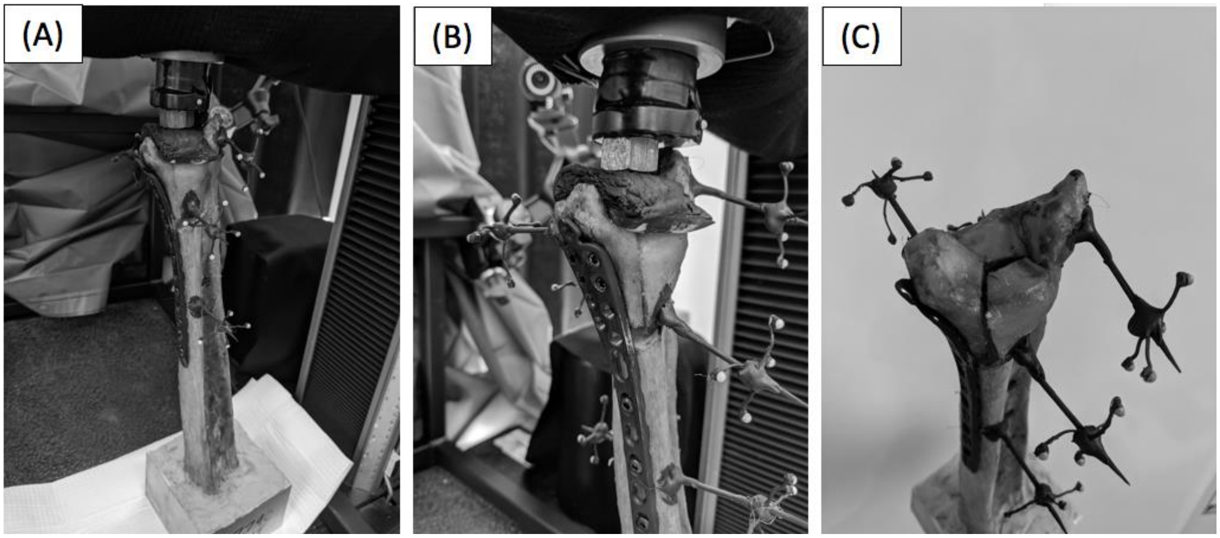

Figure F.3: Specimen 4 (Right) Failure Testing.
(A) Anterior view of initial position of the specimen (B) Anterior view of final position of the specimen (C) Posterior view of fragment failure.

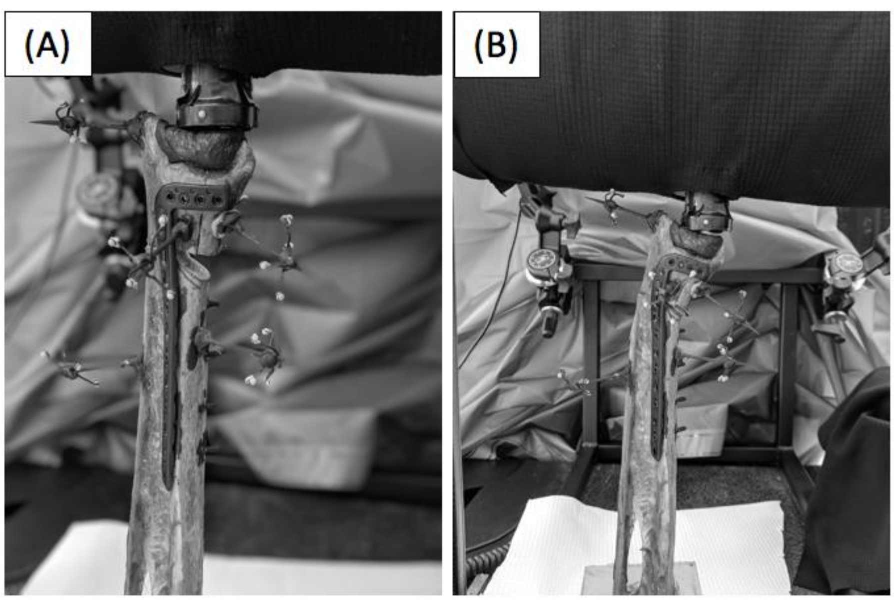

Figure F.4: Specimen 4 (Left) Failure Testing.
(A) Anterior view of initial position of the specimen (B) Anterior view of final position of the specimen.

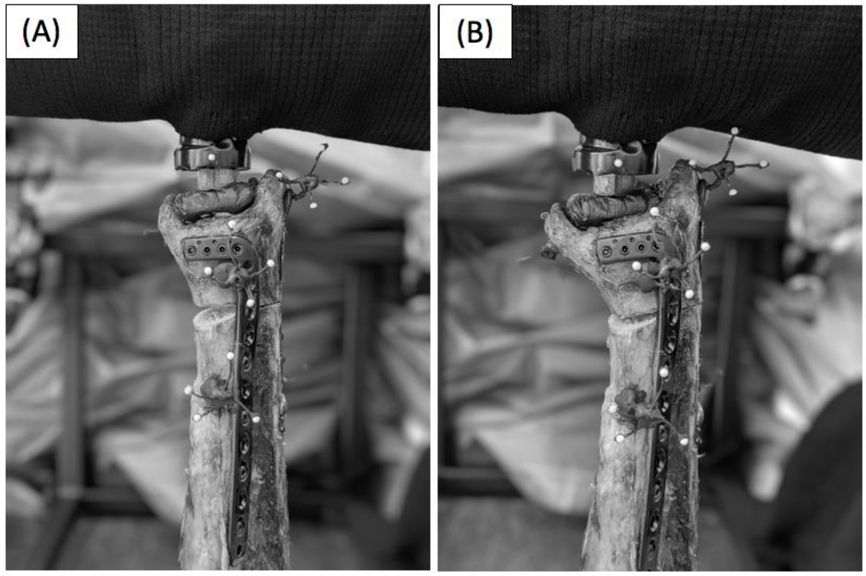

Figure F.5: Specimen 5 (Right) Failure Testing.
(A) Anterior view of initial position of the specimen (B) Anterior view of final position of the specimen.

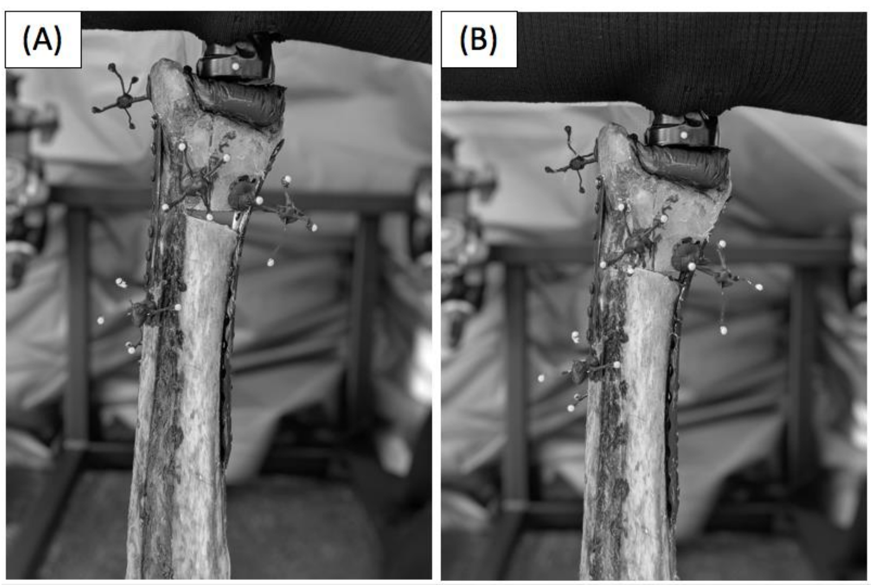

Figure F.6: Specimen 5 (Left) Failure Testing.
(A) Anterior view of initial position of the specimen (B) Anterior view of final position of the specimen.

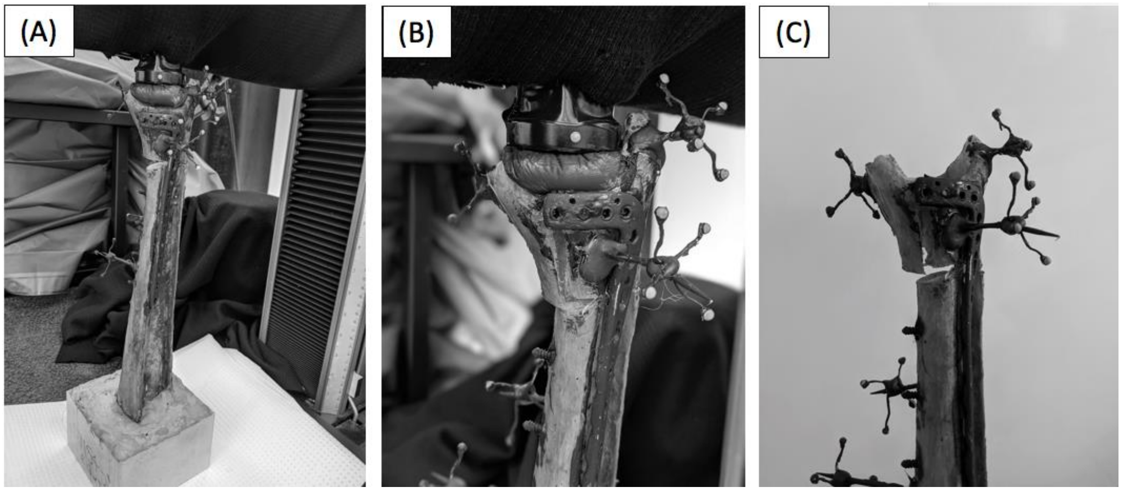

Figure F.7: Specimen 6 (Right) Failure Testing.
(A) Anterior view of initial position of the specimen (B) Anterior view of final position of the specimen (C) Posterior view of fragment failure.

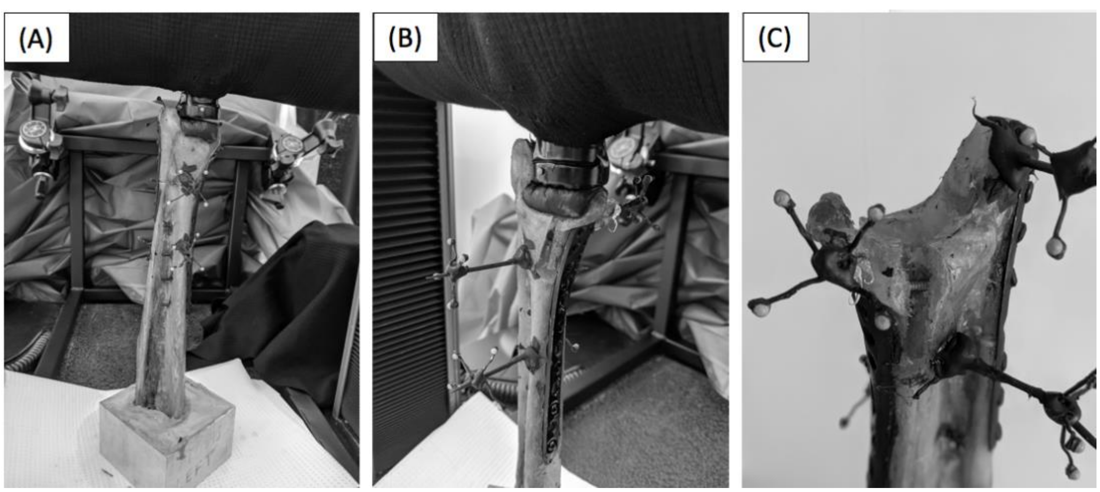

Figure F.8: Specimen 6 (Left) Failure Testing.
(A) Anterior view of initial position of the specimen (B) Anterior view of final position of the specimen (C) Posterior view of fragment failure.

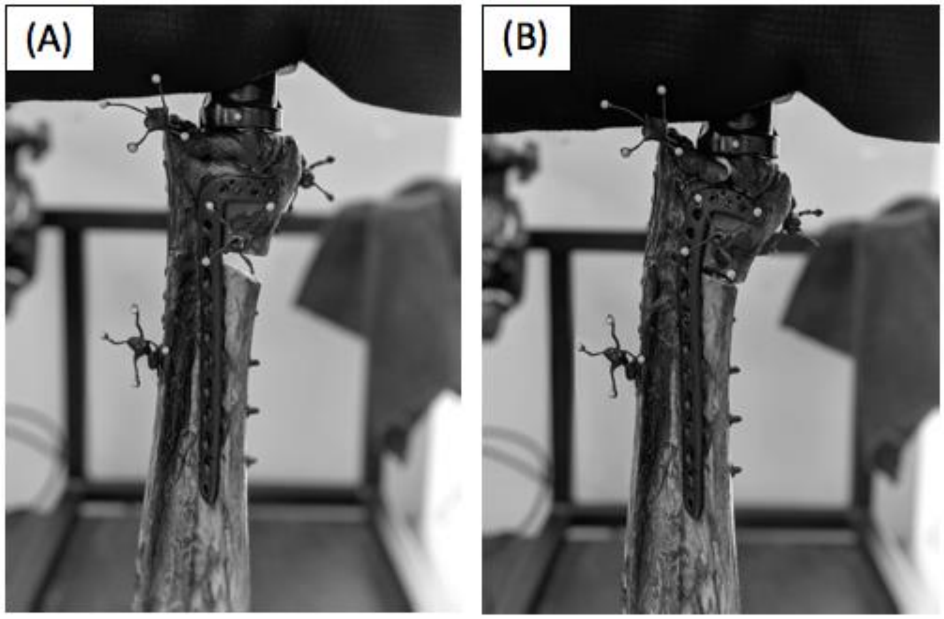

Figure F.9: Specimen 7 (Left) Failure Testing.
(A) Anterior view of initial position of the specimen (B) Anterior view of final position of the specimen.

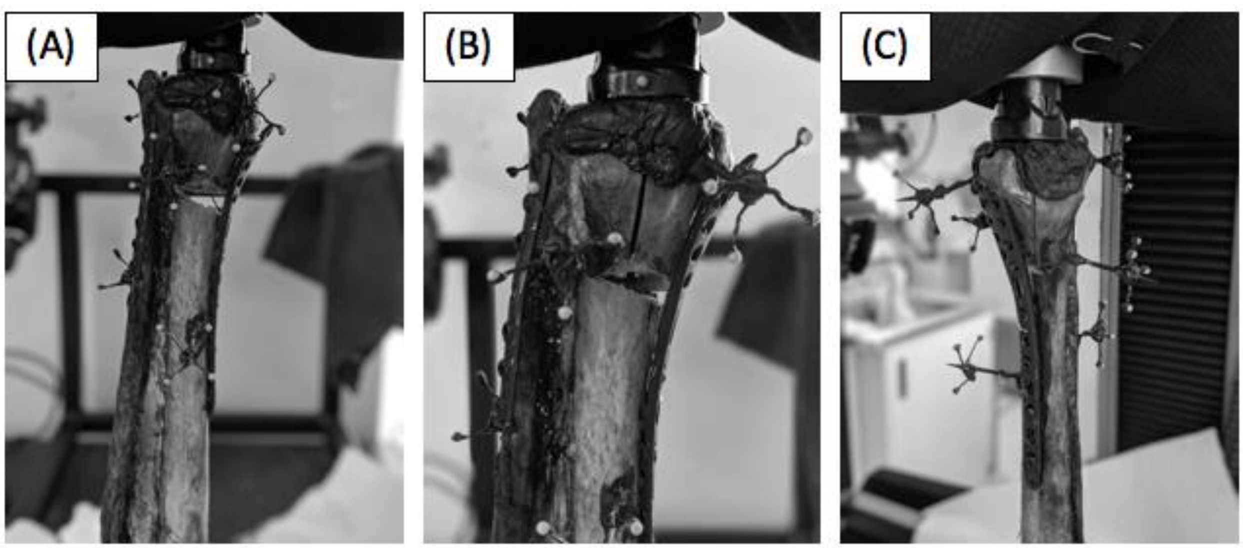

Figure F.10: Specimen 7 (Right) Failure Testing.
(A) Posterior view of the initial position of the specimen (B) Posterior view of the final position of the specimen (C) Anterior view of final position of the specimen.

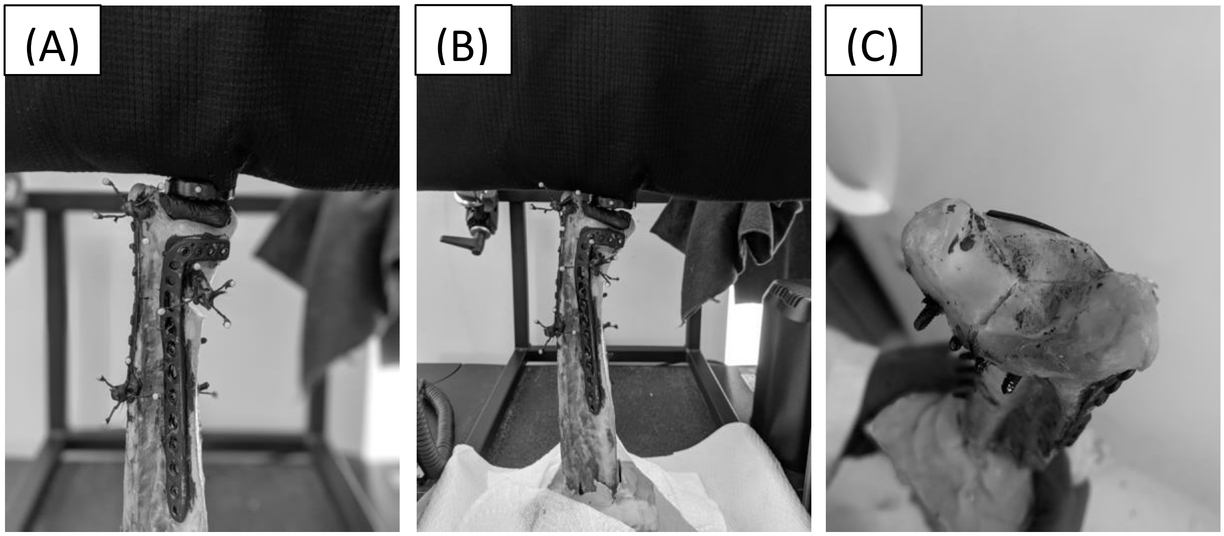

Figure F.11: Specimen 8 (Left) Failure Testing.
(A) Initial position of the specimen (B) Final position of the specimen (C) View of the articular surface of the distal tibia after failure testing.

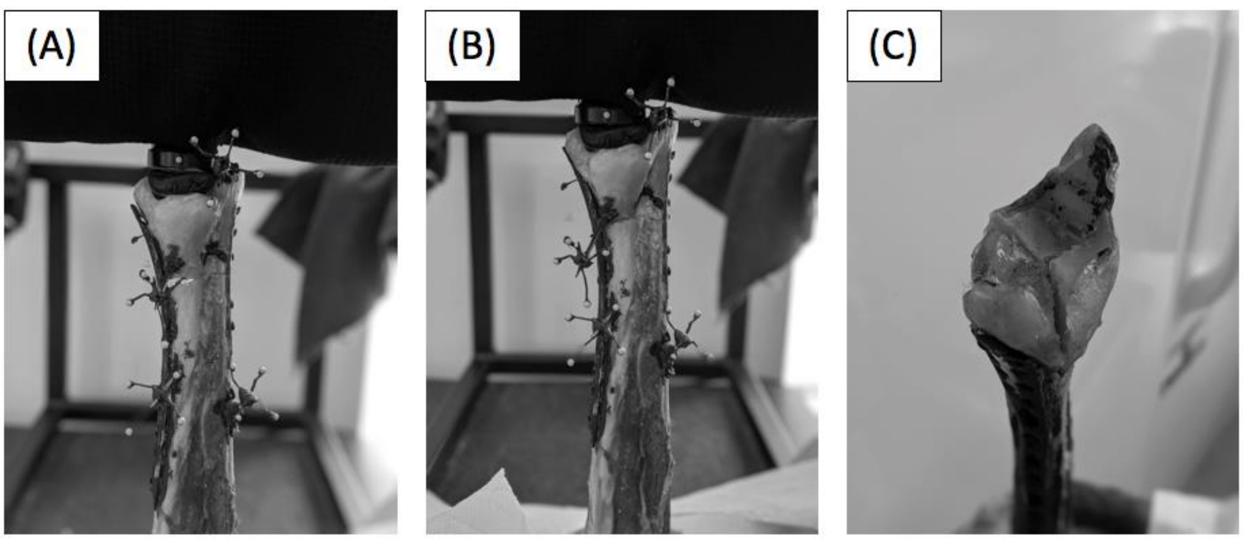

Figure F.12: Specimen 8 (Right) Failure Testing.
(A) Initial position of the specimen (B) Final position of the specimen (C) View of the articular surface of the distal tibia after failure testing.